Nonlinear Absorbing Cationic Iridium(III) Complexes Bearing Benzothiazolylfluorene Motif on the Bipyridine (N∧N) Ligand: Synthesis, Photophysics and Reverse Saturable Absorption

Yuhao Li, Naveen Dandu, Rui Liu, Lei Hu, Svetlana Kilina, and Wenfang Sun*

Department of Chemistry and Biochemistry, North Dakota State University, Fargo, North Dakota 58108-6050, United States

S *Supporting Information*

ABSTRACT: Four new heteroleptic cationic Ir(III) complexes bearing benzothiazolylfluorene motif on the bipyridine (N∧N) (**1** and **2**) and phenylpyridine (C∧N) (**3** and **4**) ligands are synthesized and characterized. The influence of the position of the substituent and the extent of π-conjugation on the photophysics of these complexes is systematically investigated by spectroscopic methods and simulated by time-dependent density functional theory (TDDFT). The complexes exhibit ligand-centered $^1\pi,\pi^*$ transitions with admixtures of ^{1}ILCT (π(benzothiazolylfluorene) $\rightarrow$ π^*(bpy)) and ^{1}MLCT (metal-to-ligand charge transfer) characters below 475 nm, and very weak ^{1,3}MLCT and ^{1,3}LLCT (ligand-to-ligand charge transfer) transitions above 475 nm. The emission of these complexes at room temperature in CH_2Cl_2 solutions is ascribed to be predominantly from the ^{3}MLCT/^{3}LLCT states for **1** and from the $^3\pi,\pi^*$ state for **2**, while the emitting state of **3** and **4** are assigned to be an admixture of ^{3}MLCT, ^{3}LLCT, and $^3\pi,\pi^*$ characters. The variations of the photophysical properties of **1−4** are attributed to different degrees of π-conjugation in the bipyridine and phenylpyridine ligands induced by different positions of the benzothiazolylfluorenyl substituents on the bipyridine ligand and different extents of π-conjugation in the phenylpyridine ligands, which alters the energy and lifetime of the lowest singlet and triplet excited states. **1−4** all possess broadband transient absorption (TA) upon nanosecond laser excitation, which extends from the visible to the NIR region. Therefore, **1−4** all exhibit strong reverse saturable absorption (RSA) at 532 nm for ns laser pulses. However, the TA of complexes **1**, **2**, and **3** are much stronger than that of **4**. This feature, combined with the difference in ground-state absorption and triplet excited-state quantum yield, result in the difference in RSA strength, which follows this trend: **1 ≈ 2 ≈ 3 > 4**. Therefore, complexes **1−3** are strong reverse saturable absorbers at 532 nm and could potentially be used as broadband nonlinear absorbing materials.

KEYWORDS: *iridium complex, synthesis, photophysics, luminescence, nonlinear optics*
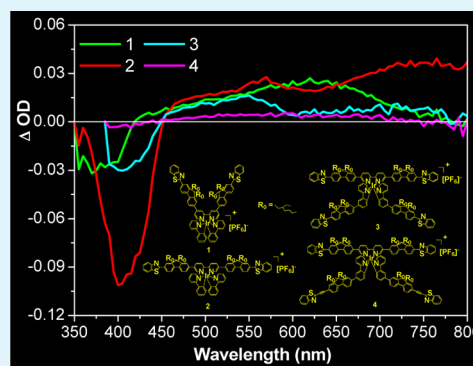
INTRODUCTION

In recent decades, coordination complexes have been the subject of extensive studies, which include square-planar d^8 complexes of Pt(II),[1−6] Pd(II),[7−9] Au(III),[10−12] and octahedral d^6 and d^7 complexes of Ru(II),[13−15] Rh(III),[16,17] Os(II),[18−20] and Ir(III)[21−24] etc. Among these transition-metal complexes, iridium(III) complexes are particularly interesting because of their strong spin−orbit coupling, which gives rise to efficient intersystem crossing and high phosphorescence efficiency. Because of these characteristics, Ir(III) complexes have been widely studied for organic light-emitting devices (OLEDs),[22,25−27] light-emitting electrochemical cells (LEECs),[28−30] luminescent biological-labeling reagents,[31−33] chemosensors,[34−36] and upconversion applications.[37]
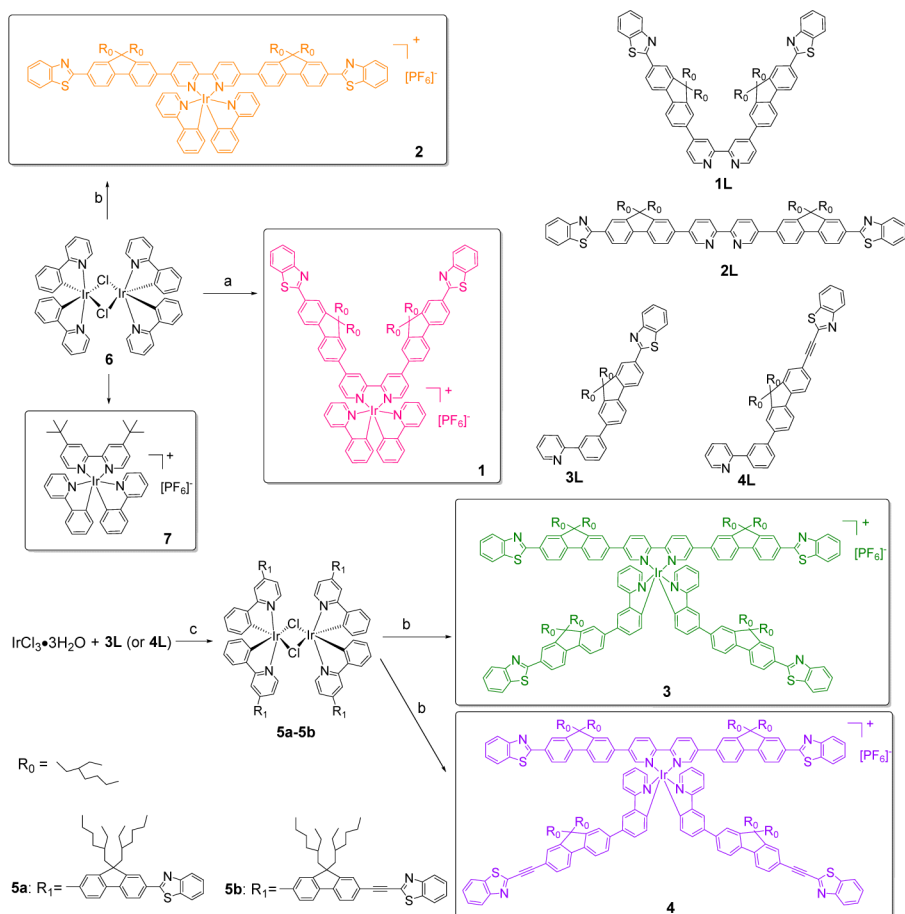
It has been well understood that the emission of the heteroleptic cationic Ir(III) complexes containing cyclometalated ligands 2-phenylpyridine (ppy, C∧N ligand) and ancillary ligands 2,2′-bipyridine (bpy, N∧N ligand) could be readily tuned by modification of the ppy or bpy ligands with electron-donating or electron-withdrawing groups.[38−42] Exploration of

the cationic Ir(III) complexes with extended π-conjugation on the ancillary diimine ligands has also been reported recently. Schanze group[43] revealed that the lowest triplet excited state of Ir(ppy)$_2$(OAE)$^+$ complexes (where OAE is a π-conjugated oligo(aryleneethynylene) substituted bpy ligand) changed from metal-to-ligand charge transfer (^{3}MLCT) state to substituted bpy ligand-based $^3\pi,\pi^*$ state when the π-conjugation of the bpy ligand was extended. Bryce and co-workers[44] reported that introducing π-conjugated fluorenyl substituent to the 3,8-position of the phenanthroline ligand in the cationic Ir(III) complexes Ir(ppy)$_2$(phen)$^+$ (phen =3,8-disubstituted phenanthroline) could increase the phosphorescence lifetime. In this case, the substitute would adjust the energy of the lowest unoccupied molecular orbitals (LUMO) and admix the ^{3}MLCT and phenanthroline ligand-based $^3\pi,\pi^*$ manifolds because of close proximity of these states. Schanze group[45] also reported a

Scheme 1. Synthetic Route for Ir(III) Complexes 1–4[a]

[a](a) (i) Ligand **1L**, CH$_3$OCH$_2$CH$_2$OH, reflux, 24 h; (ii) rt, NH$_4$PF$_6$ aq, 30 min; (b) (i) Ligand **2L**, CH$_3$OCH$_2$CH$_2$OH, reflux, 24 h; (ii) rt, NH$_4$PF$_6$ aq, 30 min; (c) CH$_3$CH$_2$CH$_2$OH, H$_2$O, reflux, 24 h.

cationic Ir(III) complex with 4-(N,N-dihexylaniline)ethynyl substituent on 5,5′-position of the bpy ligand, which exhibits a long-lived triplet excited state with strong excited-state absorption.

Although the published results[21–45] on Ir(III) complexes are intriguing, there is still no complete understanding of the effects of the π-conjugated substituent at the diimine ligand or at the cyclometalated ligand on the characteristics of the lowest singlet- and triplet-excited states in Ir(III) complexes. Particularly, with π-conjugated substituents attached on both the diimine ligand (N∧N ligand) and cyclometalated ligands (C∧N ligands), the nature of the lowest singlet- and triplet-excited states could vary from a mixed MLCT and LLCT (ligand-to-ligand charge transfer) characters to ligand-localized π,π* states or even mix all these excited states in proximity.

In addition, most of the applications reported so far primarily utilize the emission properties of the Ir(III) complexes.[22,25–37] Exploration of the nonlinear optical properties of the Ir(III) complexes and applications based on the nonlinear absorption have been rarely reported. Recently, Roberto, Angelis and co-workers reported the second harmonic generation of some cyclometalated Ir(III) complexes with substituted 1,10-phenanthroline ligand and found that both the substituents on the phenanthroline ligand and the degree of π-conjugation in the cyclometalated C∧N ligand had some influence on the second-order nonlinear optical properties of the investigated Ir(III) complexes.[46,47] Schanze group discovered that the

cationic Ir(III) complex with 5,5′-bis(4-(N,N-dihexylaniline)-ethynyl)-2,2′-bipyridine ligand displayed nonlinear absorption via a "dual-mode" two-photon absorption (TPA) and reverse saturable absorption (RSA) mechanism, demonstrating the feasibility of using Ir(III) complexes as nonlinear absorbing materials.[45] However, the influence of structural modification on the nonlinear absorption of Ir(III) complexes has not been explored. In order to optimize the nonlinear absorption of Ir(III) complexes, structure–property correlations have to be understood. Because nonlinear absorption is closely related to the ground- and excited-state properties of the complexes, such as the ground-state absorption, the excited-state energy level and decay characteristics, and the excited-state absorption, the photophysics of the interested Ir(III) complexes has to be systematically investigated via UV–vis, emission, and transient absorption spectroscopic methods. The RSA could be demonstrated via nonlinear transmission technique. The linear optical properties could be further studied via theoretical simulations to get insights into the nature of optical transitions in Ir(III) complexes and their dependence on ligand modifications.

In this paper, we report the synthesis, photophysics, and reverse saturable absorption of four cationic Ir(III) complexes **1–4** in solutions (the schematic structures are shown in Scheme 1). In addition, the optical spectra of **1–4** are simulated using time dependent density functional theory (TDDFT) to provide additional insights into the nature of

optical transitions of these complexes. To aid in our understanding of the nature of the lowest excited states in **1−4**, optical spectra of their corresponding ligands (**1L−4L**) are used as references. Complex **7** that was reported in the literature[41,48,49] is also investigated as a reference in order to evaluate the effects of extended π-conjugation in the bipyridine and 2-phenylpyridine ligands on the photophysics and reverse saturable absorption of the Ir(III) complexes. We selected benzothiazol-2-yl (BTZ) as the end-capping substituent and fluorene as the π-conjugated linker because our previous study[2] demonstrated that a Pt(II) diimine complex with 2-(benzothiazol-2′-yl)-9,9-diethyl-7-ethynylfluorene ligands exhibited very strong nonlinear absorption in the visible to the near-IR spectral region, with extremely high ratios of the excited-state to ground-state absorption cross sections and large two-photon absorption cross sections. Motivated by this study, complexes **1** and **2** were synthesized to understand how the position of substituent influences the π-conjugation on the bipyridine ligand. Complexes **3** and **4** were designed to compare the effect of extended π-conjugation on C∧N ligand. All these structural variations are expected to influence the ground- and exited-states characteristics, which would affect the photophysical properties and nonlinear absorption of these complexes.

■ EXPERIMENTAL SECTION

Synthesis and Characterization. All solvents and reagents for synthesis were obtained from Aldrich or Alfa-Aesar and used as received unless otherwise stated. Precursors 2-(benzothiazol-2′-yl)-7-bromo-9,9-bis(2-ethylhexyl)fluorene (**8**) and 2-bromo-9,9-bis(2-ethylhexyl)-7-iodofluorene (**10**) were prepared following the literature procedures,[50] by substituting ethylbromide with 2-ethylhexylbromide. 2-(3-Bromophenyl)pyridine (**13**),[51] [Ir(ppy)$_2$Cl]$_2$ (**6**),[52] and complex [(4,4′-bis(*tert*-butyl)-2,2′-bpy)(ppy)$_2$Ir]PF$_6$ (**7**)[41] were synthesized according to the literature procedures. All the solvents for spectroscopic study were HPLC grade and were obtained from Alfa Aesar Co. Ltd. and used without further purification. Tetrahydrofuran (THF), triethylamine (TEA) were distilled under N$_2$ over sodium benzophenone ketyl. Silica gels (230−400 mesh) for chromatography were from Sorbent Technology. ^{1}H NMR, HRMS and elemental analyses were used to characterize the ligands and the Ir(III) complexes. A Varian Oxford-400 VNMR spectrometer or a Varian Oxford-500 VNMR spectrometer was used to obtain the ^{1}HNMR spectra, with CDCl$_3$ or DMSO-d_6 being used as the solvent and tetramethylsilane as the internal standard. ESI-HRMS analyses were carried out on a Bruker BioTOF III mass spectrometer. Elemental analyses were conducted by NuMega Resonance Laboratories, Inc. in San Diego, California.

Synthesis of 9. Compound **8** (4.38 g, 7.27 mmol) was dissolved in degassed dry THF (60 mL). A hexane solution of *n*-BuLi (2.5 M, 3.20 mL, 7.99 mmol) was then added dropwise at −78 °C under argon atmosphere in approximately 30 min. The mixture was stirred at −78 °C for 1.5 h, then 2-isopropyl-4,4,5,5-tetramethyl-1,3,2-dioxaborolane (ITDB) (2.22 mL, 10.9 mmol) was added. The mixture was slowly warmed up to room temperature and stirred for overnight. Then 50 mL NH$_4$Cl aqueous solution was added and the mixture was stirred at rt for 0.5 h. The organic layer was separated and the aqueous layer was extracted twice with 50 mL of CH$_2$Cl$_2$. The combined organic layer was dried over MgSO$_4$. After removal of the solvent, the crude product was purified by column chromatography (silica gel), with mixed hexane/CH$_2$Cl$_2$ (v/v = 6:1 to 1:1) being used as the eluent to afford 1.90 g pale yellow oil (yield: 40%). ^{1}H NMR (400 MHz, CDCl$_3$): δ = 8.13−8.05 (m, 3H), 7.91−7.84 (m, 4H), 7.73 (d, *J* = 7.6 Hz, 1H), 7.48 (t, *J* = 7.8 Hz, 1H), 7.36 (t, *J* = 7.8, 1H), 2.07 (d, *J* = 4.8 Hz, 4H), 1.36 (s, 12H), 0.88−0.65 (m, 22H), 0.59−0.49 (m, 8H). ESI-HRMS: *m/z* calcd for (M + H)$^+$, 650.4205; found, 650.4152.

Synthesis of 1L. Compound **9** (0.20 g, 3.08 mmol), 4,4′-dibromo-2,2′-bipyridine (0.44 g, 1.40 mmol) and Pd(PPh$_3$)$_4$ (0.16 g, 0.14 mmol) were added to 30 mL of toluene. Then 7 mL of 2 M K$_2$CO$_3$ aqueous solution was added. The mixture was reacted at refluxing temperature under argon protection for 48 h. After that, the volume of the reaction mixture was reduced in vacuo and the residue was extracted with CH$_2$Cl$_2$. The CH$_2$Cl$_2$ layer was washed with brine and the combined organic layer was dried over MgSO$_4$. After the solvent was removed, the residue was purified by Al$_2$O$_3$ gel column chromatography, with mixed hexane/ethyl acetate (v/v = 15:1 to 10:1) being used as the eluent. Another column chromatographic (silica gel) purification using hexane/acetone (v/v = 6:1) as the eluent afforded 0.50 g white solid as the product (yield: 30%). ^{1}H NMR (400 MHz, CDCl$_3$): δ = 9.85 (d, *J* = 7.2 Hz, 2H), 8.26−8.12 (m, 8H), 7.79−7.92 (m, 6H), 7.84−7.79 (m, 6H), 7.54 (t, *J* = 6.2 Hz, 2H), 7.43 (t, *J* = 6.2 Hz, 2H), 2.24−2.10 (m, 8H), 0.92−0.75 (m, 32H), 0.64−0.54 (m, 28H). Anal. Calcd (%) for C$_{82}$H$_{94}$N$_4$S$_2$: C, 82.09; H, 7.90; N, 4.67. Found: C, 81.87; H, 8.38; N, 4.27. ESI-HRMS: *m/z* calcd for (M + H)$^+$, 1199.6947; found, 1199.6938.

Synthesis of 2L. Compound **9** (39.8 mg, 0.61 mmol), 5,5′-dibromo-2,2′-bipyridine (90 mg, 0.29 mmol) and Pd(PPh$_3$)$_4$ (33 mg, 0.029 mmol) were added to 20 mL of toluene. Then 2 M K$_2$CO$_3$ aqueous solution (1.45 mL) was added. The mixture was reacted at refluxing temperature under argon protection for 48 h. After that, the volume of the reaction mixture was reduced in vacuo and the residue was extracted with CH$_2$Cl$_2$. The CH$_2$Cl$_2$ layer was washed with brine and the combined organic layer was dried over MgSO$_4$. After the solvent was removed, the residue was purified by Al$_2$O$_3$ gel column chromatography by using hexane/ethyl acetate (v/v = 15:1 to 10:1) as the eluent to afford 0.11 g off-white powder (yield: 32%) as the product. ^{1}H NMR (400 MHz, CDCl$_3$): δ = 8.99 (d, *J* = 2.4 Hz, 1H), 8.56 (dd, *J*$_1$ = 8.2 Hz, *J*$_2$ = 2.4 Hz, 1H), 8.16−8.06 (m, 4H), 7.92−7.83 (m, 3H), 7.69−7.66 (m, 2H), 7.49 (t, *J* = 7.8 Hz, 1H), 7.37 (t, *J* = 7.6 Hz, 1H), 2.19−2.06 (m, 4H), 0.84−0.79 (m, 16H), 0.63−0.50 (m, 14H). Anal. Calcd for C$_{82}$H$_{94}$N$_4$S$_2$: C, 82.09; H, 7.90; N, 4.67. Found: C, 82.43; H, 8.23; N, 4.62. ESI-HRMS: *m/z* calcd for (M + H)$^+$, 1199.6947; found, 1199.6993.

Synthesis of 11. Compounds **10** (6.56 g, 11.04 mmol), Pd(PPh$_3$)$_2$Cl$_2$ (0.387 g, 0.55 mmol), PPh$_3$ (0.145 g, 0.55 mmol), and CuI (0.105 g, 0.55 mmol) were dissolved in triethylamine (40 mL) and THF (40 mL) under Ar, then trimethylsilylacetylene (1.73 mL, 1.19 g, 12.1 mmol) was added. The mixture was reacted at 30 °C for 48 h and then was concentrated in vacuo. The residue was extracted with CH$_2$Cl$_2$. The CH$_2$Cl$_2$ layer was washed with brine and the combined organic layer was dried over MgSO$_4$. After the solvent was removed, the residue was purified by silica gel column chromatography by using hexane as the eluent to afford 4.00 g product as yellow oil (yield: 64%). ^{1}H NMR (400 MHz, CDCl$_3$): δ = 7.56 (dd, *J*$_1$ = 8.4 Hz, *J*$_2$ = 2.0 Hz, 1H), 7.51−7.47 (m, 2H), 7.44−7.41 (m, 3H), 1.99−1.90 (m, 4H), 0.90−0.70 (m, 22H), 0.54−0.49 (m, 8H), 0.26 (s, 9H).

Synthesis of 12. Compound **11** (4.0 g, 7.09 mmol) was dissolved in degassed anhydrous THF (30 mL). Then a hexane solution of *n*-BuLi (2.5 M, 3.2 mL, 7.8 mmol) was added dropwise at −78 °C under Ar. The reaction mixture was stirred at this temperature for 90 min, and then ITDB (2.17 mL, 8.2 mmol) was added dropwise. The mixture was slowly warmed up to room temperature and stirred for overnight. Then 50 mL of saturated NH$_4$Cl aqueous solution was added, and the mixture was stirred at rt for 0.5 h. The mixture was extracted with CH$_2$Cl$_2$, and the CH$_2$Cl$_2$ layer was washed with brine and dried over MgSO$_4$. After removal of the solvent, the residue was purified by silica gel column chromatography by using hexane:CH$_2$Cl$_2$ (v/v = 10:1) as the eluent to afford 2.86 g colorless oil (yield: 66%). ^{1}H NMR (400 MHz, CDCl$_3$): δ = 7.80 (d, *J* = 6.8 Hz, 1H), 7.75 (d, *J* = 7.6 Hz, 1H), 7.62 (t, *J* = 9.0 Hz, 2H), 7.45−7.40 (m, 2H), 2.14−1.88 (m, 4H), 1.34 (s, 12H), 0.92−0.42 (m, 30H), 0.25 (s, 9H). ESI-HRMS: *m/z* calcd for (M+H)$^+$, 613.4614; found, 613.4481.

Synthesis of 3L. Compound **9** (1.16 g, 1.78 mmol), compound **13** (0.42 g, 1.78 mmol), and Pd(PPh$_3$)$_4$ (0.103 g, 0.089 mmol) were added to 40 mL of toluene, then 4.0 mL of 2 M K$_2$CO$_3$ aqueous

solution was added. The reaction mixture was reacted at refluxing temperature under argon protection for 48 h. After the solvent was removed, the residue was extracted with CH_2Cl_2. The CH_2Cl_2 layer was washed with water and dried over $MgSO_4$. Then the solvent was removed and the residue was purified by silica gel column chromatography by using hexane:ether (v/v = 9:1) as the eluent to afford 0.35 g colorless oil (yield = 29%). ^1H NMR (400 MHz, $CDCl_3$): δ = 8.72 (d, J = 4.8 Hz, 1H), 8.25 (t, J = 5.2 Hz, 1H), 8.14−8.01 (m, 3H), 7.96 (d, J = 8.0 Hz, 1H), 7.89 (d, J = 8.0 Hz, 1H), 7.82−7.77 (m, 4H), 7.66 (d, J = 6.8 Hz, 3H), 7.56 (t, J = 7.6 Hz, 1H), 7.47 (t, J = 7.6 Hz, 1H), 7.36 (t, J = 7.2 Hz, 1H), 7.27−7.23 (m, 1H), 2.18−2.04 (m, 4H), 0.89−0.75 (m, 17H), 0.61−0.48 (m, 13H). ESI-HRMS: m/z calcd for $(M + H)^+$, 677.3924; found, 677.3786.

Synthesis of 14. Compound **12** (0.96 g, 1.57 mmol), compound **10** (0.365 g, 1.57 mmol), and $Pd(PPh_3)_4$ (0.11 g, 0.094 mmol) were added to 30 mL of toluene, and then 4.0 mL of 2 M K_2CO_3 aqueous solution was added. The mixture was reacted at refluxing temperature under argon protection for 48 h. After the solvent was removed, the residue was extracted with CH_2Cl_2. The CH_2Cl_2 layer was washed with water and dried over $MgSO_4$. After removal of the solvent, the residue was purified by silica gel column chromatography by using hexane/ethyl acetate (v/v = 10:1) as the eluent to afford yellow oil 0.44 g (yield = 44%). ^1H NMR (400 MHz, $CDCl_3$): δ = 8.71 (d, J = 4.0 Hz, 1H), 8.23 (s, 1H), 7.95 (d, J = 8.0 Hz, 1H), 7.77 (s, 3H), 7.72 (d, J = 7.6 Hz, 1H), 7.63 (t, J = 9.4 Hz, 4H), 7.55 (t, J = 7.8 Hz, 1H), 7.45 (q, J = 11.6 Hz, 2H), 2.06−1.94 (m, 4H), 0.95−0.70 (m, 20H), 0.59−0.50 (m, 10H), 0.26 (s, 9H).

Synthesis of 15. Compound **14** (0.44 g, 0.69 mmol) was dissolved in a mixed solvent of CH_2Cl_2 (30 mL) and MeOH (30 mL), then K_2CO_3 (0.48 g, 3.46 mmol) was added. The reaction mixture was stirred at room temperature for 4 h. The solid was removed by filtration, and the filtrate was diluted with CH_2Cl_2, washed with brine and the combined organic layer was dried over $MgSO_4$. After the solvent was removed, the crude product was purified by silica gel column chromatography by using hexane:ethyl acetate (v/v = 20:1 to 10:1) as the eluent to afford 0.35 g pale yellow oil (yield: 94%). ^1H NMR (400 MHz, $CDCl_3$): δ = 8.71 (d, J = 4.8 Hz, 1H), 8.23 (s, 1H), 7.95 (d, J = 8.0 Hz, 1H), 7.77 (s, 3H), 7.72 (d, J = 7.6 Hz, 1H), 7.63 (t, J = 9.4 Hz, 4H), 7.55 (t, J = 7.8 Hz, 1H), 7.45 (q, J = 11.6 Hz, 2H), 3.09 (s, 1H), 2.06−1.94 (m, 4H), 0.95−0.70 (m, 20H), 0.59−0.50 (m, 10H). ESI-HRMS: m/z calcd for $(M + H)^+$, 568.3938; found, 568.3891.

Synthesis of 4L. Compound **15** (0.362 g, 0.638 mmol), 2-bromobenzothiazole (0.135 g, 0.638 mmol), $Pd(PPh_3)_2Cl_2$ (26.8 mg, 0.038 mmol), PPh_3 (8.36 mg, 0.032 mmol), and CuI (6.1 mg, 0.032 mmol) were mixed in triethylamine (20 mL) and THF (20 mL) at an Ar atmosphere. The mixture was reacted at 50 °C for 48 h. The volume of the reaction mixture was then reduced in vacuo, and extracted with CH_2Cl_2. The CH_2Cl_2 layer was washed by brine and then dried over $MgSO_4$. After removal of the solvent, the crude product was purified by silica gel column chromatography by using hexane:ethyl acetate (v/v = 15:1 to 12:1) as the eluent to afford 0.23 g colorless oil (yield = 51%). ^1H NMR (400 MHz, $CDCl_3$): δ = 8.72 (d, J = 4.8 Hz, 1H), 8.24 (s, 1H), 8.07 (d, J = 8.0 Hz, 1H), 7.96 (d, J = 8.0 Hz, 1H), 7.87 (d, J = 8.0 Hz, 1H), 7.78−7.73 (m, 5H), 7.68−7.62 (m, 5H), 7.58−7.49 (m, 2H), 7.43 (t, J = 7.4 Hz, 1H), 2.12−1.96 (m, 4H), 0.95−0.68 (m, 20H), 0.59−0.51 (m, 10H). ESI-HRMS: m/z calcd for $(M + H)^+$, 701.3924; found, 701.3920.

Synthesis of Complex 1. Dimeric Ir(III) complex $[(ppy)_2IrCl]_2$ (**6**) (35.3 mg, 0.033 mmol) and ligand **1L** (79.1 mg, 0.066 mmol) were suspended in 15 mL of 2-methoxyethanol. The reaction mixture was reacted at refluxing temperature under an Ar atmosphere for 24 h. After most of the solvent was removed by vacuum evaporation, the resulting concentrated solution was poured into an aqueous NH_4PF_6 solution and stirred at rt for 30 min. An orange precipitate was collected by filtration and was purified by silica gel column chromatography by using CH_2Cl_2/hexane (v/v = 1:0 to 3:1) as the eluent. The resultant solid was washed with hexane and then dried to afford 90 mg orange solid (yield = 74%). ^1H NMR (500 MHz, $CDCl_3$): δ = 8.80 (s, 1H), 8.17−8.13 (m, 3H), 8.02 (d, J = 8.5 Hz,

3H), 7.94 (d, J = 8.0 Hz, 2H), 7.90 (d, J = 8.0 Hz, 1H), 7.80 (s, 3H), 7.74 (d, J = 7.0 Hz, 1H), 7.65 (s, 1H), 7.52 (t, J = 7.8 Hz, 1H), 7.41 (t, J = 7.5 Hz, 1H), 7.15 (s, 1H), 7.08 (t, J = 8.8 Hz, 1H), 6.97 (s, 1H), 6.39 (s, 1H), 2.17−2.11 (m, 4H), 0.96−0.66 (m, 17H), 0.66−0.42 (m, 13H). Anal. Calcd for $C_{104}H_{110}F_6IrN_6PS_2$: C, 67.69; H, 6.01; N, 4.55. Found: C, 67.22; H, 6.43; N, 4.57. ESI-HRMS: m/z calcd for $(M − PF_6)^+$, 1699.7866; found, 1699.7859.

Synthesis of Complex 2. Dimeric Ir(III) complex $[(ppy)_2IrCl]_2$ (**6**) (44.7 mg, 0.042 mmol) and ligand **2L** (100 mg, 0.083 mmol) were suspended in 15 mL of 2-methoxyethanol. The reaction was carried out at refluxing temperature under an Ar atmosphere for 24 h. After most of the solvent was removed by vacuum evaporation, the resulting concentrated solution was poured into an aqueous NH_4PF_6 solution and stirred at rt for 30 min. An orange precipitate was collected by filtration and was purified by silica gel column chromatography by using CH_2Cl_2:hexane (v/v = 1:0 to 3:1) as the eluent. The resultant solid was washed with hexane and dried to afford 131 mg orange solid (yield = 84%). ^1H NMR (500 MHz, $CDCl_3$): δ = 8.85 (d, J = 8.0 Hz, 2H), 8.50 (d, J = 8.0 Hz, 2H), 8.35 (s, 2H), 8.16−8.11 (m, 6H), 7.99−7.94 (m, 4H), 7.84−7.78 (m, 9H), 7.74−7.72 (m, 2H), 7.58−7.48 (m, 3H), 7 42 (t, J = 7.5 Hz, 2H), 7 21 (t, J = 7.5 Hz, 3H), 7.11−7.07 (m, 5H), 6.51 (t, J = 6.8 Hz, 2H), 2.20−2.12 (m, 4H), 2.02−1.96 (m, 4H), 0.98−0.38 (m, 60H). Anal. Calcd for $C_{104}H_{110}F_6IrN_6PS_2$: C, 67.69; H, 6.01; N, 4.55. Found: C, 67.34; H, 6.40; N, 4.62. ESI-HRMS: m/z calcd for $(M − PF_6)^+$, 1699.7866; found, 1699.7854.

Synthesis of Complex 3. (a) Ligand **3L** (240 mg, 0.35 mmol) and $IrCl_3 \cdot 4H_2O$ (62 mg, 0.18 mmol) were added to a mixture of methoxyethanol and water (15 mL, v/v = 3:1). The reaction was carried out at refluxing temperature under an Ar atmosphere for 24 h. After it was cooled to room temperature, the mixture was extracted with CH_2Cl_2. The CH_2Cl_2 layer was washed with H_2O and dried with anhydrous $MgSO_4$. The crude product was purified by silica gel column chromatography with ethyl acetate:hexane (v/v = 1:3) being used as the eluent to afford 80 mg yellow solid (complex **5a**, yield: 15%). (b) Complex **5a** (45.7 mg, 0.014 mmol) and ligand **2L** (34.7 mg, 0.028 mmol) were suspended in 15 mL of 2-methoxyethanol. The reaction was carried out at refluxing temperature under an Ar atmosphere for 24 h. After most of the solvent was removed by vacuum evaporation, the resulting concentrated solution was poured into an aqueous NH_4PF_6 solution and stirred at r.t. for 30 min. The precipitate was collected by filtration and was purified by silica gel column chromatography with ethyl acetate:hexane (v/v = 1:10 to 1:3) being used as the eluent. The resultant solid was washed with hexane to afford 30 mg orange solid (yield = 74%). ^1H NMR (400 MHz, $CDCl_3$): δ = 8.89 (s, 1H), 8.48 (d, J = 6.0 Hz, 2H), 8.16−8.05 (m, 8H), 7.91−7.62 (m, 11H), 7.50−7.35 (m, 7H), 7.11 (d, J = 6.8 Hz, 1H), 6.59 (s, 1H), 2.13−1.90 (m, 8H), 0.83−0.34 (m, 60H). Anal. Calcd for $C_{176}H_{196}F_6IrN_8PS_4$: C, 73.17; H, 6.84; N, 3.88. Found: C, 73.40; H, 7.22; N, 4.03. ESI-HRMS: m/z calcd for $(M − PF_6)^+$, 2743.4128; found, 2743.4151.

Synthesis of Complex 4. (a) Ligand **4L** (123 mg, 0.17 mmol) and $IrCl_3 \cdot 4H_2O$ (31 mg, 0.09 mmol) were added to a mixture of methoxyethanol and water (15 mL, v/v = 3:1). The reaction was carried out at refluxing temperature under an Ar atmosphere for 24 h. After it was cooled to room temperature, the mixture was extracted with CH_2Cl_2. The CH_2Cl_2 layer was washed with H_2O and dried with anhydrous $MgSO_4$. The crude product was purified by silica gel column chromatography with ethyl acetate:hexane (v/v = 1:2) being used as the eluent to afford 37 mg yellow solid (complex **5b**, yield: 14%). (b) Complex **5b** (30 mg, 0.009 mmol) and ligand **2L** (22.1 mg, 0.018 mmol) were suspended in 15 mL of 2-methoxyethanol. The reaction was carried out at refluxing temperature under an Ar atmosphere for 24 h. After most of the solvent was removed by vacuum evaporation, the resulting concentrated solution was poured into an aqueous NH_4PF_6 solution and stirred at r.t. for 30 min. The precipitate was collected by filtration and was purified by silica gel column chromatography with ethyl acetate:hexane (v/v = 1:10 to 1:1) being used as the eluent. The resultant solid was washed with hexane to afford 20 mg dark yellow solid (yield = 76%). ^1H NMR (500 MHz, $CDCl_3$): δ = 8.93 (s, 1H), 8.75 (s, 1H), 8.52 (s, 1H), 8.26−8.11 (m,

5H), 7.99−7.85 (m, 4H), 7.81−7.40 (m, 16H), 7.14 (s, 1H), 6.35 (s, 1H), 2.26−1.82 (m, 8H), 1.08−0.35 (m, 60H). Anal. Calcd for $C_{176}H_{196}F_6IrN_8PS_4 \cdot CH_2Cl_2 \cdot H_2O$: C, 71.51; H, 6.63; N, 3.69. Found: C, 71.35; H, 6.72; N, 3.97. ESI-HRMS: *m/z* calcd for $(M - PF_6)^+$, 2791.4128; found, 2791.4155.

Photophysical Study. A Shimadzu UV-2501 spectrophotometer was used to measure the UV−vis absorption spectra of **1L−4L**, **1−4**, and **7** in different solvents. A Horiba Jobin Yvon FluoroMax-4 spectrofluorometer was used to obtain the steady-state emission spectra. The relative actinometry[53] method was utilized to measure the emission quantum yields of complexes **1−4** in degassed solutions, in which a degassed $[Ru(bpy)_3]Cl_2$ aqueous solution ($\Phi_{em} = 0.042$, $\lambda_{ex} = 436$ nm)[54] was used as the reference. An Edinburgh LP920 laser flash photolysis spectrometer pumped with the third harmonic output (355 nm) of a Nd:YAG laser (Quantel Brilliant, pulsewidth ∼4.1 ns, repetition rate is set to 1 Hz) was used to measure the nanosecond transient difference absorption spectra, the triplet excited-state lifetimes and the triplet excited-state quantum yields. All sample solutions were purged with Argon for 30 min before each measurement.

The triplet excited-state molar extinction coefficients (ε_T) at the TA band maximum was measured by the singlet depletion method;[55] and the triplet excited-state quantum yield was deduced by the relative actinometry.[56] The details of the methods were described previously.[57]

Nonlinear Transmission Measurement. The nonlinear transmission experiments at 532 nm for complexes **1−4** and **7** were conducted using a Quantel Brilliant 4.1 ns laser with a repetition rate of 10 Hz. **1−4** was measured in toluene solutions with a linear transmission of 80% in the 2-mm cuvette at 532 nm, while **3** and **7** was compared in CH_2Cl_2 solutions with a linear transmission of 85% due to the limited solubility of **7**. The experimental details were described previously.[57] The beam waist at the focal plane was approximately 96 μm (radius).

Computational Methods. All calculations, including ground state geometry optimization and excited state modeling, were performed using Gaussian 09 software package.[58]

The geometry of all the complexes at their singlet ground state was optimized using hybrid Perdew, Burke and Ernzerhof functional (PBE1)[59,60] and LANL2DZ basis set[61] assigned for Ir(III) ion and 6-31G* basis set[62−66] assigned for all other atoms. All calculations, including geometry optimization, were performed in solvent using the Conductor Polarized Continuum Model (CPCM)[67,68] as implemented in Gaussian 09. Dichloromethane (CH_2Cl_2) was chosen as the solvent for consistency with the experimental studies. Implementation of solvent also helps to avoid any unnatural charge transfer states within the energy gap of these complexes.[69] Methyl groups were used to replace the branched alkyl groups on the fluorene motifs in **1−4** to reduce computational time, since side chains have negligible effect on the electronic structure of the complexes. The optimized geometries of complexes **1−4** are reported in the Supporting Information Table S1.

Linear response TDDFT calculations were performed to determine the optical spectra of complexes **1−4** using the same functional, basis sets, and solvent model as for geometry optimization. For obtaining the absorption spectra, 50 lowest singlet transitions were calculated, from which the vertical excitation energies at the ground state optimal geometry were obtained. These transition energies were plotted as peaks in the absorption spectra (see Figure 1c). To match with the experimental data in Figure 1b, a line-width of 0.1 eV was used to broaden each spectral line obtained from the TDDFT calculations.

Emission energies for the complexes **1−4** were calculated by optimizing their geometries at their singlet and triplet excited states with analytic TDDFT[70] calculations utilizing the same methodology as for absorption spectra calculations. This approach provided the vertical transition energies of the lowest singlet and triplet excited states at its optimal geometry. To determine the charge transfer behavior in the absorption and emission transitions, natural transition orbitals (NTOs)[71] were computed by applying the unitary transformation that diagonalizes the transition density matrix obtained from TDDFT calculations and represents the electron excitation as a single-particle electron−hole pair. As incorporated in Gaussian 09 software package,
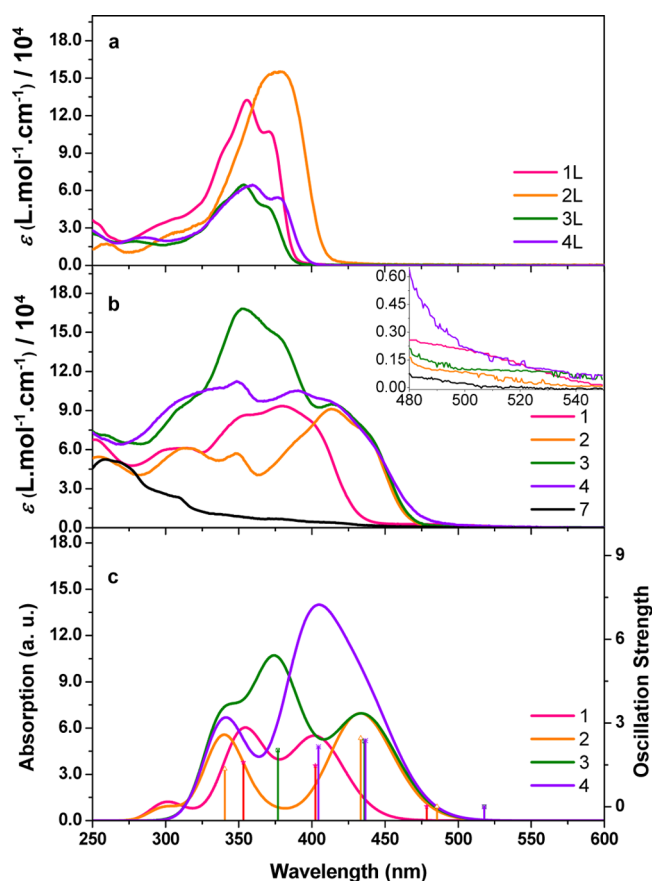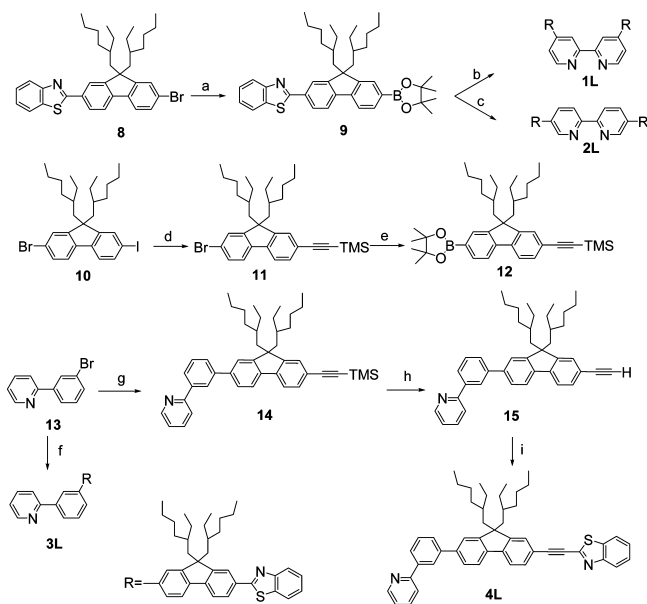

Figure 1. (a) UV−vis absorption spectra of **1L-4L** in CH_2Cl_2. (b) Experimental UV−vis absorption spectra of **1−4** and **7** in CH_2Cl_2. (c) Calculated UV−vis absorption spectra for complexes **1−4** in CH_2Cl_2.

this approach allows depicting each optical transition between the ground and excited states as a single-particle transition from an occupied (hole) orbital to an unoccupied (electron) orbital. As such, NTOs characterize the excited state via excited orbitals of an electron (to which an electron is excited) and hole (from which an electron is transferred). In contrast to the ground-state molecular orbitals (MOs) obtained from DFT calculations, electron and hole NTOs calculated from TDDFT represent the *excited state* electronic density, which includes excitonic effects such as an electron−hole correlation; therefore, is a widely used method for characterization of charge transfer properties of the excited state of various metal−organic complexes.[72−74] All NTOs are visualized using cubegen function, with the isovalue of 0.02 as provided in the GaussView 5.1 graphical software.[75]

RESULTS AND DISCUSSION

Molecular Design and Synthesis. The synthetic routes for complexes **1−4** and the respective ligands **1L−4L** are illustrated in Schemes 1 and 2. Benzothiazolylfluorene group was introduced to 2,2′-bipyridine ligand at different positions in order to tune both the ground-state and excited-state properties. Branched alkyl chains were attached on the 9-position of fluorene motif to prevent the intermolecular interactions and improve the solubility of the Ir(III) complexes. Suzuki coupling reaction was used to couple benzothiazolyl-fluorene motif to bpy or ppy ligands to obtain ligands **1L−4L** at a yield varying from 29% to 44%. Sonogashira coupling reaction was utilized to incorporate the C≡C triple bond between the benzothiazole and fluorene motifs for extending the π-conjugation, and the yield was approximately 50%.

6560

dx.doi.org/10.1021/am401133p | ACS Appl. Mater. Interfaces 2013, 5, 6556−6570

Scheme 2. Synthetic Route for Ligands 1L−4L[a]

[a](a) (i) BuLi, −78 °C, Ar, 1.5 h; (ii) ITDB, −78 °C, Ar, 1.5 h then rt 12 h; (b) 4,4′-dibromo-2,2′-bipyridine, Pd(PPh₃)₄, K₂CO₃, H₂O, toluene, Ar, reflux, 48 h; (c) 5,5′-dibromo-2,2′-bipyridine, Pd(PPh₃)₄, K₂CO₃, H₂O, toluene, Ar, reflux, 48 h; (d) trimethylsilylacetylene, THF, TEA, Pd(PPh₃)₂Cl₂, PPh₃, CuI, Ar, rt, 48 h; (e) (i) BuLi, −78 °C, Ar, 1.5 h; (ii) ITDB, −78 °C, Ar, 1.5 h then rt 12 h; (f) compound (9), Pd(PPh₃)₄, K₂CO₃, H₂O, toluene, Ar, reflux, 48 h; (g) compound (12), Pd(PPh₃)₄, K₂CO₃, H₂O, toluene, Ar, reflux, 48 h; (h) K₂CO₃, CH₂Cl₂, MeOH, rt, 4 h; (i) 2-bromobenzothiazole, THF, TEA, Pd(PPh₃)₂Cl₂, PPh₃, CuI, Ar, 50 °C, 48 h.

The synthetic procedure for the cationic Ir(III) complexes **1−4** follows two steps. First, the chloro-bridged dinuclear Ir(III) complexes **5a**, **5b**, or **6** were synthesized according to the reported method by Nonoyama.[76] Then the cationic Ir(III) complexes **1−4** were synthesized by bridge-breaking accompanied by coordination reaction with the ancillary bipyridine ligand. Compared to the reaction conditions for synthesizing neutral Ir(III) complexes, this reaction can be carried out under mild reaction conditions and reasonably high yields were obtained. All Ir(III) complexes (**1−4**) are air-stable and soluble in most organic solvents. ^{1}H NMR spectrum, elemental analysis and high-resolution mass spectrum (HRMS) confirmed the proposed structures for complexes **1−4**.

Electronic Absorption. The UV−vis absorption of ligands **1L−4L** and Ir(III) complexes **1−4** and **7** obeys Beer's law in

the concentration range of $1 \times 10^{-6}-5 \times 10^{-4}$ mol L^{-1}, suggesting the absence of ground-state aggregation in this concentration range . This should be attributed to the reduced intermolecular interactions due to the branched alkyl chains on the fluorene motif and the octahedral geometry of the Ir(III) complexes. The UV−vis absorption spectra of ligands **1L−4L** in CH₂Cl₂ are shown in Figure 1a. The maximum absorption bands between 350 and 380 nm can be characterized by the long-axis polarized $^1\pi,\pi^*$ transitions. The absorption spectrum of the linear bipyridine ligand **2L** is red-shifted compared to the V-shaped bipyridine ligand **1L**, which is due to the more delocalized electron distribution in the linear-shaped molecule. The absorption spectrum of ligand **4L** also bathochromically shifts compared to that of **3L**, attributing to the extended π-conjugation in **4L** due to the insertion of the triplet bond. The molar extinction coefficients of **1L** and **2L** approximately double those of **3L** and **4L**.

Figure 1b shows the experimental UV−vis absorption spectra of Ir(III) complexes **1−4** and **7** in CH₂Cl₂. The theoretical UV−vis spectra of **1−4** in CH₂Cl₂ continuum media obtained by TDDFT calculations are displayed in Figure 1c. The overall trends revealed in the experimental data are well reproduced in the theoretical spectra. As seen in Figure 1b, the reference complex **7** possesses strong absorption below 325 nm, which arises from $^1\pi,\pi^*$ transitions within the bpy and ppy ligands. The broad and weak tail between 350 and 500 nm can be attributed to the mixture of ^{1}LLCT (~375 nm), ^{1}MLCT (~425 nm), ^{3}LLCT, and ^{3}MLCT (~475 nm) according to the literature report.[49] In contrast to complex **7**, the UV−vis absorption spectra of **1−4** possess several major bands between 300 and 500 nm, as shown in Figure 1b and summarized in Table 1. Comparing these bands to those of their respective ligands, and considering the TDDFT calculations of NTOs contributing to these transitions (represented in Tables 2 and 3), we can make the following assignment to the major absorption bands in **1**: the strongest absorption band at ca. 380 nm and the shoulder around 350 nm predominantly arise from the bipyridine ligand based $^1\pi,\pi^*$ and ^{1}ILCT (π(BTZ-fluorene) → π*(bpy)) transitions with some contribution from the ^{1}MLCT transition (see Table 2), while the weak band between 450 and 550 nm for **1** are dominated by ^{1}LLCT/^{1}MLCT transitions (see Table 3), possibly mixed with spin-forbidden ^{3}LLCT/^{3}MLCT transitions according to that reported for reference complex **7**.[49] Note that the electron−hole NTO pairs represented in Tables 2 and 3 differ from the ground-state unoccupied and occupied MOs. Photoexcitation mixes the ground state MOs contributing to optical transitions because of

Table 1. Experimental Photophysical Data and TDDFT Calculations of the Emission Energies of 1−4

		298 K		77 K	λ_{phos}^{theor}/nm[d]	λ_{T1-Tn}/nm (τ_{TA}/μs; log ε_{T1-Tn}; Φ_T)[e]
	λ_{abs}/nm (log ε)[a]	λ_{em}/nm (τ_{em}/μs); Φ_{em}[b]		λ_{em}/nm (τ_{em}/μs)[c]		
1	314 (4.79), 355 (4.94), 379 (4.97)	582 (1.20); 0.33		550 (82.1); 595 (78.6)	591	620 (5.30; 4.98; 0.13)
2	313 (4.79), 348 (4.76), 413 (4.96), 430 (4.89)	600 (6.80); 645 (6.70); 0.097		556 (20.1); 611 (19.7)	643	735 (8.35; 4.76; 0.30)
3	307 (4.95), 353 (5.22), 378 (5.17), 414 (4.98)	608 (1.39); 655 (1.40); 0.14		567 (12.2); 612 (11.4)	650	550 (0.20; 4.65; 0.16)
4	322 (5.02), 349 (5.05), 390 (5.02), 413 (4.99)	609 (1.32); 650 (1.30); 0.027		573 (9.9); 614 (7.4)	651	590 (0.30; 5.06; 0.015)

[a]Absorption band maxima and molar extinction coefficients of the UV−vis absorption in CH₂Cl₂ at room temperature. [b]Emission band maxima and decay lifetimes in CH₂Cl₂ at room temperature, $c = 1 \times 10^{-5}$ mol/L. The reference used was a degassed aqueous solution of [Ru(bpy)₃]Cl₂ (Φ_{em} = 0.042, λ_{ex} = 436 nm). [c]Emission band maxima and decay lifetimes at 77 K in BuCN glassy matrix, $c = 1 \times 10^{-5}$ mol/L. [d]Calculated by TDDFT for optimized triplet geometry. [e]Nanosecond TA band maxima, triplet extinction coefficients, triplet excited-state lifetimes, and quantum yields measured in toluene at room temperature. SiNc in C₆H₆ was used as the reference. (ε_{590} = 70 000 L mol^{-1} cm^{-1}, Φ_T = 0.20).[77]

Table 2. Natural Transition Orbitals (NTOs) Representing Transitions Contributing to the Main Absorption Band of 1−4 in CH₂Cl₂[a]

Complex	Excited state and properties	Holes	Electrons
1	3rd excited state 402 nm $f = 1.47$		
	11th excited state 353 nm $f = 1.29$		
2	2nd excited state 433 nm $f = 2.45$		
	11th excited state 340 nm $f = 1.36$		
3	3rd excited state 437 nm $f = 2.34$		
	8th excited state 378 nm $f = 2.12$		
4	3rd excited state 436 nm $f = 2.37$		
	5th excited state 404 nm $f = 2.37$		

[a]Calculations were carried out in CH₂Cl₂ using the PBE1 functional and the LANL2DZ/6-31G* basis set. The solvent model used was the CPCM reaction field model.
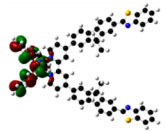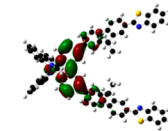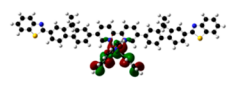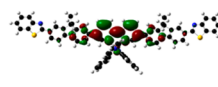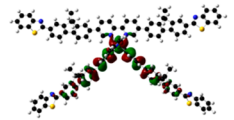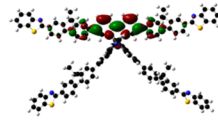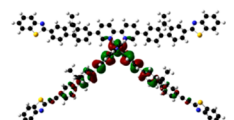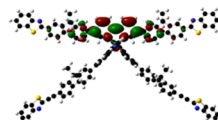
strong Coulomb interaction between a photoexcited electron and hole, that is, excitonic effect. As such, an excitonic state cannot be represented as a single pair of the ground-state MOs, while NTOs represent the excited-state density. NTOs can be considered as a weighted sum of the ground-state MOs that contribute to a given excited state, thus compactly representing the charge transfer character of an optical transition.[71]

The bathochromic shift of the major absorption bands of **1** compared to those in **1L** should be ascribed to the stabilization of the bpy ligand-based LUMO after coordination with the Ir(III) ion, which is in line with the other reported Ir(III) complexes.[39,43,45] Because of the strong $^1\pi,\pi^*$ transitions, the MLCT and LLCT transitions are buried in the experimental spectrum. However, the TDDFT calculations clearly indicate the presence of these transitions at the longer wavelength of the spectrum. Due to the strong spin−orbit coupling in third-row transition metals like iridium, the spin-forbidden triplet transitions are also possible.[39,49] For complex **2**, despite a noticeable red-shift of the spectrum, the assignments of major peaks are similar to those for complex **1**. This is because the linear-shape of the ligand in **2** favors the π-conjugation between

the bipyridine component and the BTZ-fluorene component. The increased π-conjugation decreases the energy of optical transitions, resulting in a bathochromic shift of the absorption spectrum of **2** versus **1**.

For complexes **3** and **4**, in addition to the $^1\pi,\pi^*$/^{1}ILCT transitions around 410 nm that are associated with the substituted bipyridine ligand and thus are essentially the same as that discovered in complex **2**, other strong absorption bands appear between 350 and 400 nm. According to the TDDFT calculations, these bands predominantly emanate from the $^1\pi,\pi^*$ transitions localized on the benzothiazolylfluorenyl substituted 2-phenylpyridine ligand. This assignment is supported by the similar energies of these bands to those of the $^1\pi,\pi^*$ transitions in their respective ligands **3L** and **4L** (Figure 1a). Similar to that observed from **3L** and **4L**, the inserted triple bond between benzothiazole and fluorene in complex **4** leads to the red-shift of these bands between 350 and 400 nm. The ^{1,3}MLCT/^{1,3}LLCT transitions also present at the lowest-energy range of complexes **3** and **4**, while their oscillator strengths are much weaker than those in complexes **1** and **2** (see Table 3). In addition, from the expansion of the

6562

dx.doi.org/10.1021/am401133p | ACS Appl. Mater. Interfaces 2013, 5, 6556−6570

Table 3. Natural Transition Orbitals (NTOs) Representing Transitions Contributing to the Lowest-Energy Band of 1−4 in CH_2Cl_2[a]

Complex	Excited states properties	Holes	Electrons
1	$\lambda = 478$ nm $f = 0.0031$		
2	$\lambda = 485$ nm $f = 0.0026$		
3	$\lambda = 517$ nm $f = 0.0004$		
4	$\lambda = 517$ nm $f = 0.0005$		

[a]Calculations were carried out in CH_2Cl_2 using the PBE1 functional and the LANL2DZ/6-31G* basis set. The solvent model used was the CPCM reaction field model.

spectra in the range of 480 and 540 nm (see the inset in Figure 1b) and from the TDDFT calculations (Table 3), it is apparent that the ^{1,3}MLCT/^{1,3}LLCT transitions are red-shifted in 3 and 4 compared to those in 1 and 2. This should be attributed to the increased π-conjugation of the phenylpyridine ligand in 3 and 4, which raises the energy of the substituted phenylpyridine and Ir(III) based HOMO in these two complexes.

Photoluminescence. The room-temperature emission spectra of complexes 1−4 and 7 in CH_2Cl_2 are shown in Figure 2, and the emission data of 1−4 are summarized in Table 1. For reference complex 7, the excitation wavelength was selected at its charge-transfer band of 375 nm. The excitation wavelengths of complexes 1−4 were chosen at their respective mixed $^{1}\pi,\pi*/^{1}$ILCT band around 410 nm, which

gave rise to orange-red luminescence. The emission for all complexes exhibits significant Stokes shifts of 7389−7818 cm^{-1}, and the emission lifetime in degassed CH_2Cl_2 solutions are several microseconds, which are several times longer than that for complex 7.[41] Moreover, the emission is subject to oxygen quenching as exemplified in the inset of Figure 2 for 2. The calculated energies of the triplet emission transitions are indicated by arrows in Figure 2. Remarkably, the calculated energies of the lowest-energy triplet transitions well correlate with the lowest-energy peaks of the experimental spectra. Taking all these facts into account, we assign the observed emission from complexes 1−4 to phosphorescence from a triplet excited state (T_1 excited state).

Compared to the emission of complex 7, the emission of complex 1 shows a significant red-shift of 26 nm with a broad structureless feature, while complex 2 exhibits a red-shift of 44 nm with a vibronic substructure. Complexes 3 and 4 demonstrate slight red-shifts compared to 2. According to that reported in the literature for other Ir(III) complexes,[25,38,39,78] phosphorescence spectra from the ligand-centered $^{3}\pi,\pi*$ state typically exhibit vibronic progressions with long lifetimes, while the ^{3}CT emission are broad and featureless and have shorter lifetimes. Therefore, the emission from complex 1 in CH_2Cl_2 is tentatively assigned to the ^{3}MLCT/^{3}LLCT state, while complex 2 in CH_2Cl_2 likely emits from the bipyridine ligand-centered $^{3}\pi,\pi*$ state, probably mixed with little ^{3}MLCT/^{3}ILCT characters. Complexes 3 and 4 show a weak vibronic progression but with similar lifetime to that of 1, suggesting a mixed $^{3}\pi,\pi*/^{3}$CT characters of the emitting states in CH_2Cl_2. According to our TDDFT calculations of the lowest-energy triplet transitions and related NTOs shown in Table 4, the emission of complex 1 possesses mostly ^{3}MLCT/^{3}LLCT characters, which well correlates with the featureless shape of its emission spectrum. In contrast, the lowest-energy triplet transition in complex 2 is dominated by $^{3}\pi,\pi*$ character with a small admixture of ^{3}MLCT/^{3}ILCT
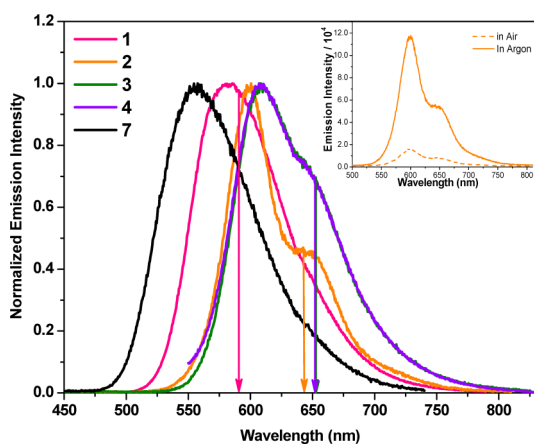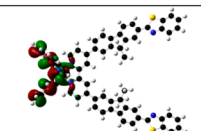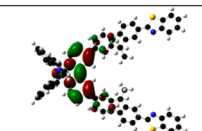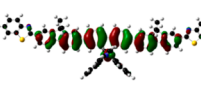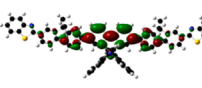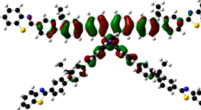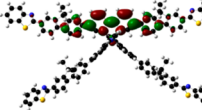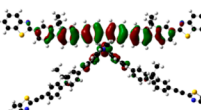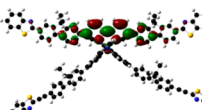

Figure 2. Normalized emission spectra of complexes 1 ($\lambda_{ex} = 400$ nm), 2 ($\lambda_{ex} = 413$ nm), 3 ($\lambda_{ex} = 418$ nm), 4 ($\lambda_{ex} = 420$ nm), and 7 ($\lambda_{ex} = 375$ nm) in CH_2Cl_2 solutions ($c = 1 \times 10^{-5}$ mol L^{-1}). The inset displays the emission spectra of complex 2 in air and argon atmospheres in CH_2Cl_2 solution ($c = 1 \times 10^{-5}$ mol L^{-1}). The arrows indicate the triplet transitions obtained from TDDFT calculations.

Table 4. NTOs Representing Transitions Corresponding to Triplet Emission of 1−4 in CH$_2$Cl$_2$ Calculated by TDDFT Method

Complex	Emission energy	Holes	Electrons
1	591 nm		
2	643 nm		
3	650 nm		
4	651 nm		
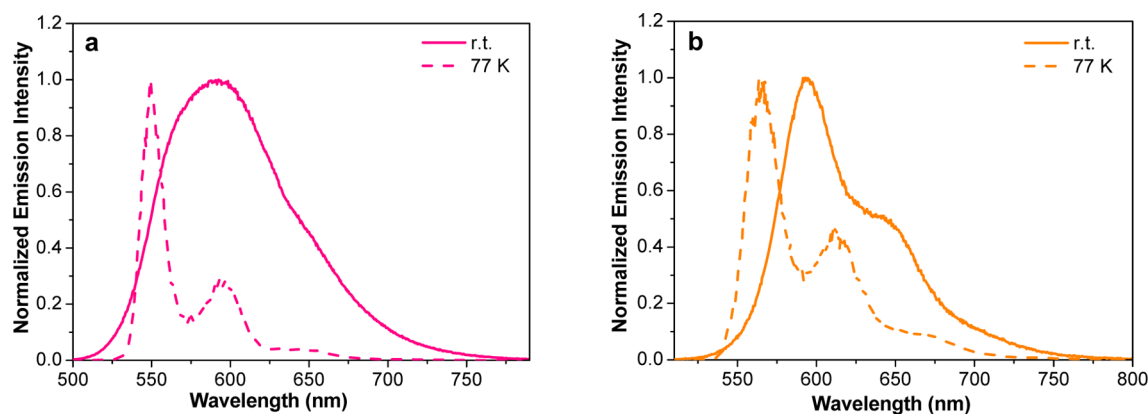
Figure 3. Emission spectra of **1** (a) (λ_{ex} = 396 nm) and **2** (b) (λ_{ex} = 418 nm) at rt and 77 K in BuCN.

characters. Complexes **3** and **4** exhibit a larger degree of mixture of the ^{3}MLCT/^{3}LLCT characters with the $^3\pi,\pi^*$ configuration in their emission compared to that in **2**, which agrees very well with our predictions based on the spectral feature and lifetime of their emissions. Therefore, the experimental findings match perfectly with the character of NTOs contributing to the triplet emission of complexes **1−4**. This analysis also clearly indicates that modification of the bipyridine ligand from nonlinear (4,4′-positions) to linear (5,5′-positions) framework diminishes the charge transfer characters in the lowest triplet excited state, while the extended π-conjugation of the phenylpyridine ligand also alters the triplet emitting excited state to mixed charge transfer and $^3\pi,\pi^*$ characters.

According to the nature of the emission discussed above, the LUMOs of complexes **1−4** are primarily located on the bipyridine ligand, which is consistent with that reported in the literature for other Ir(III) complexes.[38,39,41,42,44] The bathochromic shifts of the emission bands in complexes **1** and **2** indicate that extended π-conjugation on bipyridine ligand decreases the LUMO energy level. Complex **2** containing the linear-shaped bpy ligand has a lower LUMO than complex **1** containing the V-shaped bpy ligand due to better conjugation.

Therefore, the HOMO−LUMO gaps in **1** and **2** are reduced compared to that in **7**, resulting in the red-shifted emission in **1** and **2**. Complexes **3** and **4** exhibit slight red-shifts compared to **2** because the HOMO in **3** and **4** is slightly raised due to the delocalization of electron density on the phenylpyridine component, the Ir(III) center, and the substituted bipyridine ligand. Incorporation of the benzothiazolylfluorenyl substituent does not influence the HOMO of **3** and **4** pronouncedly because no electron density extends to this component.

Comparison of the Φ_{em} of **1** and **2** clearly shows that **1** (Φ_{em} = 0.33) is more emissive than **2** (Φ_{em} = 0.097), indicating that extended π-conjugation in the bipyridine ligand decreases the emission efficiency, which is consistent with that observed from similar complexes bearing extended π-conjugated ligand in the literature.[38,39,43,45] Complexes **3** and **4** also demonstrate the similar trend: with the extended π-conjugation in the phenylpyridine ligand, the emission efficiency of **4** decreases compared to that of **3**. The decreased emission efficiency in **2**, **3** and **4** should be attributed to the increased $^3\pi,\pi^*$ characters in the emitting state of these complexes because of the increased π-conjugation in their ligands compared to that in **1**. A previous study on homoleptic Ir(III) complexes found that the ^{3}MLCT dominated triplet excited state exhibits highly efficient

phosphorescence due to much larger radiative rate constant (k_r).[25] Some of the best yellow-to-orange emitters[21,22,25] used in single-layer OLED devices also possess ^{3}MLCT dominated emission and thus high phosphorescence quantum yields. Therefore, the diminished charge transfer character in the lowest triplet excited states of **2**−**4** reduces their emission efficiencies.

The low-temperature (77 K) photoluminescence spectra of complexes **1**−**4** in butyronitrile (BuCN) were studied and the results are summarized in Table 1. Comparisons of the spectra at room temperature and at 77 K are displayed in Figure 3 for **1** and **2** and in Supporting Information Figures S5 and S6 for **3** and **4**, respectively. The emission spectra for all complexes manifest a hypsochromic shift at 77 K and become narrower and more structured, with a thermal Stokes shift of 1179−1534 cm^{-1}. This suggests that the emission from **1**−**4** all possesses charge transfer characters. However, contributions from $^3\pi,\pi^*$ state also present in view of the nice vibronic structures.

The photoluminescence of **1**−**4** in different solvents were investigated to further understand the nature of the emission. The solvent-dependency emission spectra of **1** are manifested in Figure 4 and the spectra for **2**−**4** are provided in Supporting
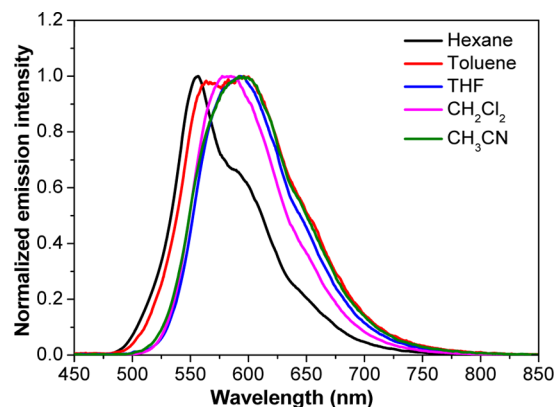

Figure 4. Normalized emission spectra of **1** in different solvents under an argon atmosphere (λ_{ex} = 436 nm).

Information Figures S7−S9. The emission energy, lifetime, and quantum yield for **1**−**4** in different solvents are compiled in Table 5. Complexes **1**, **3**, and **4** demonstrate a clear solvatochromic effect, while the solvent effect on **2** is minor. This is in line with our aforementioned assignment of the emitting states for **1**, **3**, and **4** being predominantly charge transfer in nature, while the emission being primarily from the

Table 5. Emission Parameters of 1−4 in Different Solvents at rt

	λ_{em}/nm (τ_{em}/μs; Φ^a)				
	hexane^b	toluene	THF	CH$_2$Cl$_2$	CH$_3$CN
1	555 (11.9; 0.35)	565 (5.13; 0.21)	594 (0.877; 0.25)	582 (1.20; 0.33)	595 (0.96; 0.22)
2	590 (12.1; 0.068)	588 (8.36; 0.080)	600 (5.97; 0.11)	600 (6.80; 0.097)	594 (5.47; 0.096)
3	630 (0.49; 0.018)	655 (0.20; 0.011)	620 (0.55; 0.06)	608 (1.39; 0.14)	621 (0.53; 0.039)
4	620 (0.26; 0.006)	634 (0.093; 0.007)	613 (0.43; 0.01)	609 (1.32; 0.027)	609 (0.51; 0.008)

^{a}The reference used was a degassed aqueous solution of [Ru(bpy)$_3$]-Cl$_2$ (Φ_{em} = 0.042, λ_{ex} = 436 nm). ^{b}With ~10% CH$_2$Cl$_2$.

$^3\pi,\pi^*$ for **2**. To quantitatively inspect the relationship of the emission energy and solvents polarity, $E_T(30)$ values[79] for different solvents are used and the correlation plots are shown in Figure 5. When the $E_T(30)$ value of solvent increases, the

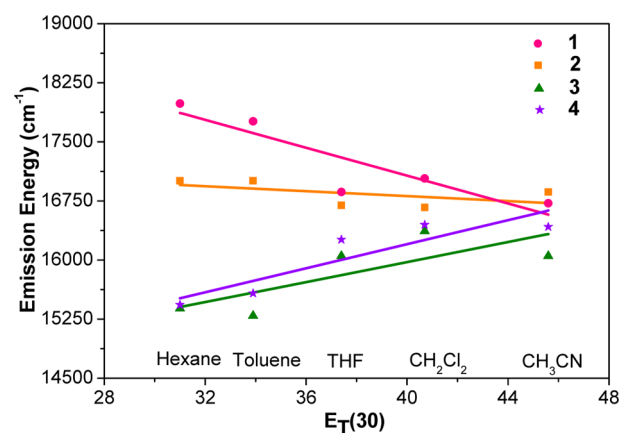**Figure 5.** Correlation diagram of the emission energy vs solvent $E_T(30)$ values for **1**−**4**.

emission energy (E_{em}) of **1** decreases pronouncedly, clearly a positive solvatochromic effect. In contrast, a negative solvatochromic effect is observed for **3** and **4**, implying a less polar emitting excited state than the ground state. This again supports the notion that the emitting states of **3** and **4** contain a significant charge transfer character. However, the positive solvatochromic effect observed from **1** is contrary to the characteristic of ^{3}MLCT/^{3}LLCT emission (which typically exhibits a negative solvatochromic effect) assigned for **1** earlier. A close examination of the shape of the emission spectra and the lifetimes of **1** in hexane and toluene solutions reveals that the emission spectra in these two solvents possess salient vibronic structures and is much more long-lived than the emission in polar solvents. This implies that unlike the ^{3}MLCT/^{3}LLCT emission in polar solvents, the emission of **1** in nonpolar solvents like hexane and toluene is dominated by the ligand-localized $^3\pi,\pi^*$ emission. This could explain the unusual positive solvatochromic effect observed for **1**. Solvent-induced switch of the emitting state has been found for Pt(II) diimine complexes before.[2,80]

On top of the aforementioned solvatochromic effect, the emission lifetime (τ_{em}) and quantum yield (Φ_{em}) are also affected by the different solvents significantly. As demonstrated in Supporting Information Figure S10, the emission quantum yields of **1**−**4** (Φ_{em}) roughly correlate with their emission energy (E_{em}) in each solvent used. With an increase of E_{em}, the Φ_{em} increase, which is consistent with reported work for homoleptic Ir(III) complexes.[25] In noncoordinating solvents such as CH$_2$Cl$_2$, the emission lifetime becomes longer and the quantum yield is increased in comparison to those in coordinating solvents like CH$_3$CN, which further supports the notion of admixing ^{3}MLCT configuration in the emitting state in these complexes. This phenomenon is common for transition-metal complexes with a ^{3}MLCT emitting state.[81]

Transient Difference Absorption. Transient difference absorption (TA) spectroscopy is another powerful tool for studying the excited-state characteristics, which measures the difference of the excited-state absorption and the ground-state absorption. By monitoring the decay of the TA, the lifetime of the excited state contributing to the TA can be obtained.
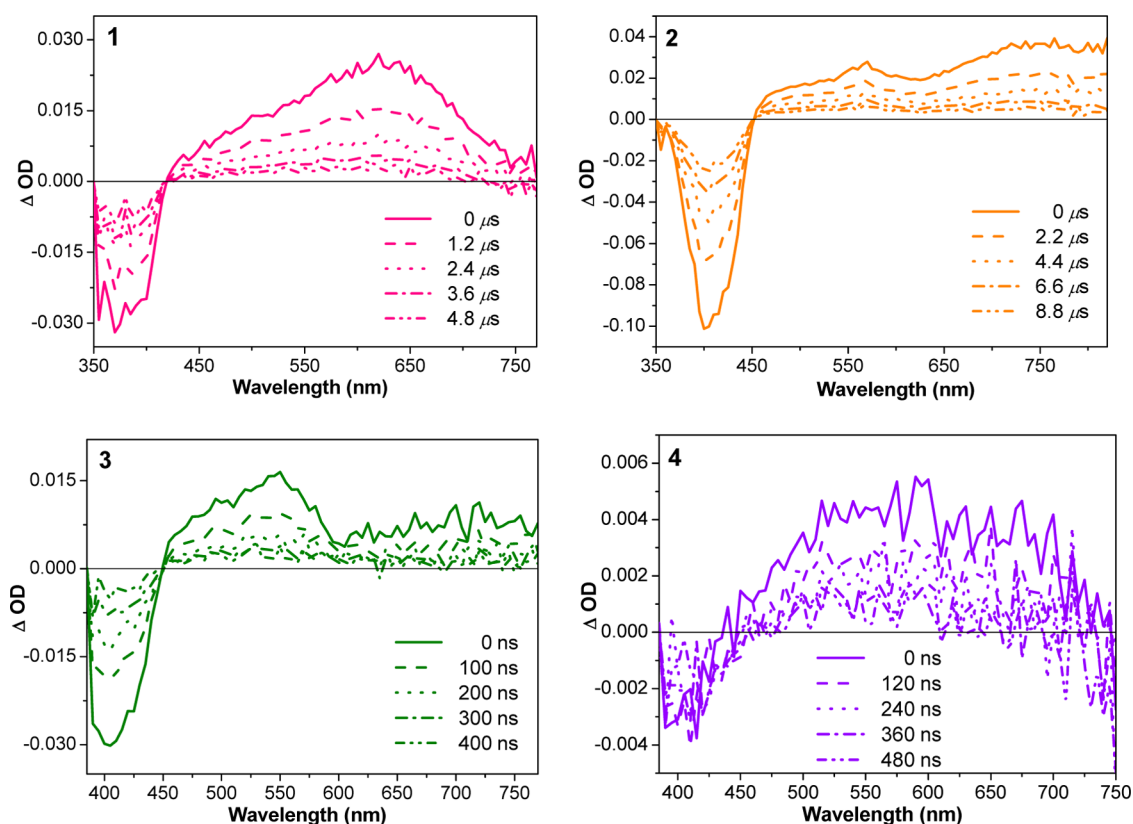
Figure 6. Time-resolved triplet TA spectra of **1**−**4** in toluene solution. λ_{ex} = 355 nm, A_{355} = 0.4 in a 1-cm cuvette.

Previous studies on some Ir(III) complexes revealed that those complexes possess broad triplet excited-state absorption extending from the visible to the near-IR region.[43,45,82,83] The emission study on **1**−**4** also suggests long-lived triplet excited states of these complexes. As a result, we anticipate to observe the triplet excited-state absorption from **1**−**4**. Figure 6 demonstrates the time-resolved triplet TA spectra of **1**−**4** upon excitation at 355 nm at room temperature in deaerated toluene solutions (toluene was chosen as the solvent instead of CH_2Cl_2 because of the better stability of the toluene solution than the CH_2Cl_2 solution upon laser irradiation). The TA parameters for these complexes are summarized in Table 1.

The TA spectra of these complexes are quite distinct. **1** features a ground-state bleaching at ~375 nm and a strong absorption band that extends from 425 to 750 nm. **2** exhibits a red-shifted bleaching at ~400 nm compared to **1**, which is consistent with their respective UV−vis absorption band maximum, and a broad, strong absorption band from 450 nm and extending into the near-infrared region. The lifetimes deduced from the decay of the TA (shown in Table 1) are in accordance with those obtained from the emission decay in toluene (see Table 5), suggesting the same parentage of the absorbing excited state and the emitting excited state for **1** and **2** in toluene. On the basis of the nature of the emitting states assigned to these two complexes in toluene, and with reference to the previous reports on d^6 and d^7 transition metal complexes with π-conjugated ligands,[43,45,82,84] we tentatively attribute the excited states giving rise to the observed TA of **1** and **2** in toluene to predominantly $^3\pi,\pi^*$ excited states. The TA lifetimes of **3** and **4** are quite similar to those obtained from their emission decay and they are much shorter than those for **1** and **2**. This implies that the excited states leading to the TA spectra

of **3** and **4** should have the mixed ^{3}LLCT/^{3}MLCT/$^3\pi,\pi^*$ characters in nature.

It should be noted that the triplet quantum yields (Φ_T) listed in Table 1 for **1**−**4** are significantly lower than unity, which is typically assumed for Ir(III) complexes due to the largest spin−orbit coupling constant in Ir(III) complexes. The low triplet quantum yield could be accounted for by three factors: First, the triplet quantum yield was measured by relative actinometry,[56] in which the optical density change (ΔOD) of the Ir(III) complex at its TA band maximum is compared to the ΔOD of the reference compound SiNc at its TA band maximum measured at optically matched solutions at identical experimental conditions. This lays a limitation that the measured Φ_T from this method only reflects the excited state giving rise to TA. It is reported that intersystem crossing of some Ru(II) complexes can populate both the ^{3}MLCT and $^3\pi,\pi^*$ states.[85−87] If only one of these states exhibits transient absorption, then the measured Φ_T by this method would be smaller than the actual intersystem crossing yield. We assume that this phenomenon applies to the Ir(III) complexes discussed here. Second, it has been reported for Pt(II) complexes that the increased π-conjugation in the ligand decreases the spin−orbit coupling,[88] which in turn reduces the triplet quantum yield. Third, the calculation of triplet quantum yield uses the triplet molar extinction coefficient obtained by the singlet depletion method,[55] which assumes negligible triplet absorption at the bleaching wavelength and negligible ground-state absorption at the TA band maximum. If the triplet absorption at the bleaching wavelength cannot be neglected, the triplet molar extinction coefficient obtained from the singlet depletion method would be overestimated. Consequently, the triplet quantum yield calculated would be underestimated. We

speculate all these factors contribute to the smaller triplet quantum yields in **1–4**. This could also explain why the emission quantum yield of **3** in toluene ($\Phi_{em} = 0.21$ in Table 5) is larger than the triplet quantum yield in toluene ($\Phi_T = 0.13$ in Table 1).

Reverse Saturable Absorption (RSA). The broad positive triplet TA band in the visible to the near-IR region for **1–4** (as shown in Figure 6) suggests stronger triplet excited-state absorption with respect to the ground-state absorption in this spectral region for these complexes. Therefore, reverse saturable absorption (RSA) (defined as the absorptivity increase or transmission decrease when the incident fluence increases) is expected to occur from these complexes under ns laser irradiation. To manifest this, nonlinear transmission experiments were conducted using 4.1 ns laser pulses at 532 nm for **1–4** in toluene solution in a 2-mm cuvette. The toluene solution of each complex was prepared to have an identical 80% linear transmission in the 2-mm cuvette for comparison purpose. To evaluate the effect of benzothiazolylfluorenyl substituent on the bipyridine and phenylpyridine ligands on the RSA of the Ir(III) complexes, the RSA of the reference complex **7** was also investigated under identical experimental conditions except that a CH_2Cl_2 solution with a 85% linear transmission in the 2-mm cuvette was used for **7**, because **7** has poor solubility in toluene to obtain the required 80% linear transmission. The transmission vs incident energy curves for **1–4** are depicted in Figure 7. All of the complexes exhibit remarkable transmission
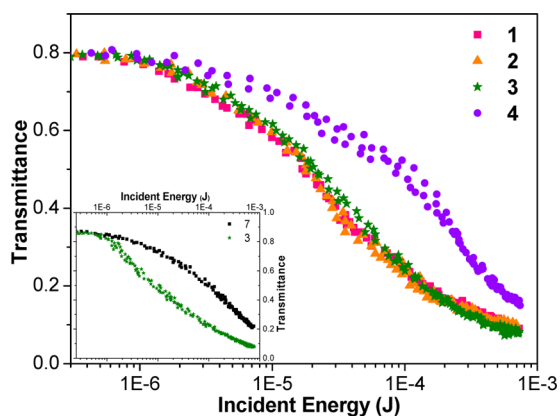

Figure 7. Transmittance vs incident energy curves for **1–4** in toluene for 4.1 ns laser pulses at 532 nm in a 2-mm cuvette. The linear transmission was adjusted to 80% for each sample in the 2-mm cell. The inset shows the comparison of **3** and **7** in CH_2Cl_2 solutions with a linear transmission of 85% in the 2-mm cell for 4.1 ns laser pulses at 532 nm.

decrease with the increased incident energy, clearly indicating the occurrence of strong RSA. The RSA of **1**, **2**, and **3** is significantly stronger than that of **4**. The RSA threshold for **1–3**, which is defined as the incident energy that reduces the transmittance to 70% of the linear transmittance, is approximately 3 μJ, and the transmission drops to 0.08 at the incident energy of 680 μJ. Comparison of the RSA of **3** to that of **7** (see the inset in Figure 7) clearly manifests that incorporation of benzothiazolylfluorenyl substituents on the bipyridine and phenylpyridine ligands drastically improves the RSA of the Ir(III) complexes.

To rationalize the observed trend of RSA for **1–4** in toluene, the ratio of the excited-state absorption cross section (σ_{ex}) relative to that of the ground-state (σ_0), which is one of the key

parameters for RSA, has to be assessed for **1–4**. According to the ε values at 532 nm, which can be obtained from the UV–vis absorption spectra (Supporting Information Figures S11–S14), and the conversion equation: $\sigma = 2303\varepsilon/N_A$ (where N_A is the Avogadro constant), the ground-state absorption cross sections (σ_0) at 532 nm for **1–4** in toluene solutions can be deduced. Using the respective ΔOD values at 532 nm and at the TA band maximum immediately after the laser excitation (which can be determined from the TA spectrum at zero delay), as well as the ε_{T1-Tn} at the TA band maximum, and applying the method reported by our group before,[89] we can estimate the triplet excited-state absorption cross sections at 532 nm. The obtained σ_0 and σ_{ex} values are listed in Table 6. The σ_0 values in

Table 6. Ground-State (σ_0) and Excited-State (σ_{ex}) Absorption Cross Sections of 1–4 in Toluene at 532 nm

	1	2	3	4
$\sigma_0/10^{-18}$ cm^2	0.157	0.222	0.704	3.97
$\sigma_{ex}/10^{-18}$ cm^2	232	124	160	547
σ_{ex}/σ_0	1478	558	228	138
$\Phi_T\sigma_{ex}/\sigma_0$	197	169	37	2.1

Table 6 clearly indicate that extending the π-conjugation on either the N∧N or the C∧N ligands significantly increases the σ_0 value at 532 nm for these complexes, consequently, the ratio of σ_{ex}/σ_0 decreases following this trend: **1 > 2 > 3 > 4**. Complexes **1** and **2** with the extended π-conjugation only on N∧N ligand show larger σ_{ex}/σ_0 ratios than complexes **3** and **4** that have the extended π-conjugation on both N∧N and C∧N ligands. Because the rapid intersystem crossing in the Ir(III) complexes, the excited state that makes the major contribution to the observed RSA should be the triplet excited state. Therefore, the triplet excited-state quantum yields (Φ_T) of **1–4** should influence the observed RSA as well. The combined $\Phi_T\sigma_{ex}/\sigma_0$ values for **1–4** are provided in Table 6. The trend of these combined values correlates with the observed RSA very well. The stronger RSA of **1**, **2**, and **3** should thus be attributed to their larger σ_{ex}/σ_0 ratios and their higher triplet quantum yields compared to those of **4** at 532 nm. It is worth noting that the estimated σ_{ex}/σ_0 value at 532 nm for **1** is larger than that for the Pt(II) bipyridyl complex bearing the benzothiazolylfluorenyl acetylide ligands reported by our group previously (σ_T/σ_0 = 1200)[2] (which was among the largest ratios reported for Pt(II) complexes at 532 nm to date),[90,91] although the σ_{ex} value obtained by the method mentioned above is only a rough estimation. Nonetheless, to the best of our knowledge, the RSA observed from **1**, **2**, and **3** is among the strongest for ns laser pulses at 532 nm considering all of the currently reported reverse saturable absorbers.[2,5,45,90−105] It should also be pointed out that although the RSA of **4** is weaker than those of **1–3**, its two-photon absorption cross sections in the near-IR region could be larger than **1–3** in view of its more extended π-conjugation in the phenylpyridine ligands. This prediction is based on our discovery from the Pt(II) complexes with more extended π-conjugated ligands via insertion of a C≡C triple bond[90,104] and will be confirmed from wavelength dispersion Z-scan study in the near future.

■ CONCLUSION

Four cationic Ir(III) complexes (**1–4**) with benzothiazolyl-fluorenyl substituent on the bipyridine and/or on the phenylpyridine ligands were synthesized. Their ground-state

and excited-state properties were systematically investigated. All complexes possess strong absorption bands below 475 nm, which predominantly originate from the ligand-based $^1\pi,\pi^*$ and ^{1}ILCT transitions, also mixed with some ^{1}MLCT characters, and weak ^{1,3}MLCT and ^{1,3}LLCT transitions above 475 nm that are buried in the strong $^1\pi,\pi^*/^1$ILCT bands. The degree of π-conjugation in both the bipyridine and phenylpyridine ligands significantly influences the $^1\pi,\pi^*/^1$ILCT transition energies. The $^1\pi,\pi^*/^1$ILCT transitions in complexes **2**-**4** that contain the linear-shaped bipyridine ligand are pronouncedly red-shifted compared to those in complex **1** with a V-shaped bipyridine ligand. Additionally, the nature of the lowest triplet excited state of these Ir(III) complexes is modulated by the degree of π-conjugation in the bipyridine and phenylpyridine ligands. The emission of **1** is dominated by ^{3}MLCT/^{3}LLCT characters, while **2** exhibits $^3\pi,\pi^*$ dominated emission in CH_2Cl_2 solutions. Complexes **3** and **4** demonstrate the mixed characters of ^{3}LLCT/^{3}MLCT/$^3\pi,\pi^*$ in their emission. The extended π-conjugation in the ligands increases the $^3\pi,\pi^*$ configuration in the lowest triplet excited state. All complexes exhibit broadband triplet excited-state absorption extending from the visible to the near-IR region, which leads to strong reverse saturable absorption (RSA) at 532 nm for ns laser pulses. Similar to the trend observed from the emission study, the different degrees of π-conjugation in the ligands alter the spectral feature of the excited-state absorption, which in turn affect the strength of RSA. The trend of RSA strength decreases as: **1** $\approx$ **2** $\approx$ **3** > **4**, which is mainly determined by the combined $\Phi_T \sigma_{ex}/\sigma_0$ values. The long-lived triplet excited state and broad triplet excited-state absorption of **1**-**4** makes them very promising candidates for photonic devices that require strong nonlinear absorption. Moreover, this study demonstrates that the RSA of the cationic Ir(III) complexes can be dramatically improved by extending the π-conjugation in the bipyridine ligand.

■ ASSOCIATED CONTENT

ⓢ Supporting Information

UV–vis absorption spectra of **1**–**4** in different solvents, emission spectra of **3** and **4** at rt and 77 K in BuCN, emission spectra of **2**–**4** in different solvents, and correlation diagram for the emission quantum yield (Φ_{em}) vs emission energy (E_{em}) in different solvents for **1**–**4**. This material is available free of charge via the Internet at http://pubs.acs.org.

■ AUTHOR INFORMATION

Corresponding Author
*E-mail: Wenfang.Sun@ndsu.edu. Phone: 701-231-6254.

Notes
The authors declare no competing financial interest.

■ ACKNOWLEDGMENTS

■ REFERENCES

(1) Huang, L.; Zeng, L.; Guo, H.; Wu, W.; Wu, W.; Ji, S.; Zhao, J. *Eur. J. Inorg. Chem.* **2011**, 4527–4533.

(2) Sun, W.; Zhang, B.; Li, Y.; Pritchett, T. M.; Li, Z.; Haley, J. E. *Chem. Mater.* **2010**, 22, 6384–6392.

(3) Huang, K.; Yang, H.; Zhou, Z.; Chen, H.; Li, F.; Yi, T.; Huang, C. *Inorg. Chim. Acta* **2009**, 362, 2577–2580.

(4) Liu, Y.; Wu, W.; Zhao, J.; Zhang, X.; Guo, H. *Dalton Trans.* **2011**, 40, 9085–9089.

(5) Pritchett, T. M.; Sun, W.; Zhang, B.; Ferry, M. J.; Li, Y.; Haley, J. E.; Mackie, D. M.; Shensky, W.; Mott, A. G. *Opt. Lett.* **2010**, 35, 1305–1307.

(6) Ni, J.; Zhang, L.; Wen, H.; Chen, Z. *Chem. Commun.* **2009**, 3801–3803.

(7) Lai, S. W.; Cheung, T. C.; Chan, M. C. W.; Cheung, K. K.; Peng, S. M.; Che, C. M. *Inorg. Chem.* **2000**, 39, 255–262.

(8) Tsubomura, T.; Ito, Y.; Inoue, S.; Tanaka, Y.; Matsumoto, K.; Tsukuda, T. *Inorg. Chem.* **2008**, 47, 481–486.

(9) Neve, F.; Crispini, A.; Di Pietro, C.; Campagna, S. *Organometallics* **2002**, 21, 3511–3518.

(10) He, X.; Yam, V. W.-W. *Inorg. Chem.* **2010**, 49, 2273–2279.

(11) Czerwieniec, R.; Hofbeck, T.; Crespo, O.; Laguna, A.; Gimeno, M. C.; Yersin, H. *Inorg. Chem.* **2010**, 49, 3764–3767.

(12) Bojan, V. R.; Lopez-de-Luzuriaga, J. M.; Manso, E.; Monge, M.; Olmos, M. E. *Organometallics* **2011**, 30, 4486–4489.

(13) Ryan, G. J.; Quinn, S.; Gunnlaugsson, T. *Inorg. Chem.* **2008**, 47, 401–403.

(14) Elmes, R. B. P.; Orange, K. N.; Cloonan, S. M.; Williams, D. C.; Gunnlaugsson, T. *J. Am. Chem. Soc.* **2011**, 133, 15862–15865.

(15) Robson, K. C. D.; Koivisto, B. D.; Gordon, T. J.; Baumgartner, T.; Berlinguette, C. P. *Inorg. Chem.* **2010**, 49, 5335–5337.

(16) Indelli, M. T.; Chiorboli, C.; Flamigni, L.; De Cola, L.; Scandola, F. *Inorg. Chem.* **2007**, 46, 5630–5641.

(17) Leung, S. K.; Kwok, K. Y.; Zhang, K. Y.; Lo, K. K. W. *Inorg. Chem.* **2010**, 49, 4984–4995.

(18) Ciofini, I.; Laine, P. P.; Bedioui, F.; Adamo, C. *J. Am. Chem. Soc.* **2004**, 126, 10763–10777.

(19) Lai, S.; Chan, Q. K. W.; Zhu, N.; Che, C. M. *Inorg. Chem.* **2007**, 46, 11003–11016.

(20) Onicha, A. C.; Castellano, F. N. *J. Phys. Chem. C* **2010**, 114, 6831–6840.

(21) Slinker, J. D.; Gorodetsky, A. A.; Lowry, M. S.; Wang, J. J.; Parker, S.; Rohl, R.; Bernhard, S.; Malliaras, G. G. *J. Am. Chem. Soc.* **2004**, 126, 2763–2767.

(22) Parker, S. T.; Slinker, J. D.; Lowry, M. S.; Cox, M. P.; Bernhard, S.; Malliaras, G. G. *Chem. Mater.* **2005**, 17, 3187–3190.

(23) Zhu, M.; Zou, J.; He, X.; Yang, C.; Wu, H.; Zhong, C.; Qin, J.; Cao, Y. *Chem. Mater.* **2012**, 24, 174–180.

(24) Song, M.; Park, J. S.; Gal, Y. S.; Kang, S.; Lee, J. Y.; Lee, J. W.; Jin, S. H. *J. Phys. Chem. C* **2012**, 116, 7526–7533.

(25) Tsuboyama, A.; Iwawaki, H.; Furugori, M.; Mukaide, T.; Kamatani, J.; Igawa, S.; Moriyama, T.; Miura, S.; Takiguchi, T.; Okada, S.; Hoshino, M.; Ueno, K. *J. Am. Chem. Soc.* **2003**, 125, 12971–12979.

(26) Du, B.; Lin, C.; Chi, Y.; Hung, J.; Chung, M.; Lin, T.; Lee, G. H.; Wong, K. T.; Chou, P. T.; Hung, W. Y.; Chiu, H. C. *Inorg. Chem.* **2010**, 49, 8713–8723.

(27) Vacca, P.; Petrosino, M.; Guerra, A.; Chierchia, R.; Minarini, C.; Della Sala, D.; Rubino, A. *J. Phys. Chem. C* **2007**, 111, 17404–17408.

(28) Sun, L.; Galan, A.; Ladouceur, S.; Slinker, J. D.; Zysman-Colman, E. *J. Mater. Chem.* **2011**, 21, 18083–18088.

(29) Zysman-Colman, E.; Slinker, J. D.; Parker, J. B.; Malliaras, G. G.; Bernhard, S. *Chem. Mater.* **2008**, 20, 388–396.

(30) Bolink, H. J.; Cappelli, L.; Coronado, E.; Gratzel, M.; Orti, E.; Costa, R. D.; Viruela, P. M.; Nazeeruddin, M. K. *J. Am. Chem. Soc.* **2006**, 128, 14786–14787.

(31) Zhao, Q.; Yu, M.; Shi, L.; Liu, S.; Li, C.; Shi, M.; Zhou, Z.; Huang, C.; Li, F. *Organometallics* **2010**, 29, 1085–1091.

(32) Xiong, L.; Zhao, Q.; Chen, H.; Wu, Y.; Dong, Z.; Zhou, Z.; Li, F. *Inorg. Chem.* **2010**, 49, 6402–6408.

(33) Li, C.; Yu, M.; Sun, Y.; Wu, Y.; Huang, C.; Li, F. *J. Am. Chem. Soc.* **2011**, 133, 11231–11239.

(34) Zhao, Q.; Cao, T. Y.; Li, F.; Li, X.; Jing, H.; Yi, T.; Huang, C. *Organometallics* **2007**, 26, 2077–2081.

(35) Zhao, Q.; Liu, S.; Shi, M.; Li, F.; Jing, H.; Yi, T.; Huang, C. *Organometallics* **2007**, 26, 5922–5930.

(36) Zhao, N.; Wu, Y.; Wen, H.; Zhang, X.; Chen, Z. *Organometallics* **2009**, *28*, 5603−5611.

(37) Sun, J.; Wu, W.; Guo, H.; Zhao, J. *Eur. J. Inorg. Chem.* **2011**, 3165−3173.

(38) Zhao, Q.; Liu, S.; Shi, M.; Wang, C.; Yu, M.; Li, L.; Li, F.; Yi, T.; Huang, C. *Inorg. Chem.* **2006**, *45*, 6152−6160.

(39) Ladouceur, S.; Fortin, D.; Zysman-Colman, E. *Inorg. Chem.* **2010**, *49*, 5625−5641.

(40) Neve, F.; La Deda, M.; Crispini, A.; Bellusci, A.; Puntoriero, F.; Campagna, S. *Organometallics* **2004**, *23*, 5856−5863.

(41) Ladouceur, S.; Fortin, D.; Zysman-Colman, E. *Inorg. Chem.* **2011**, *50*, 11514−11526.

(42) Costa, R. D.; Monti, F.; Accorsi, G.; Barbieri, A.; Bolink, H. J.; Orti, E.; Armaroli, N. *Inorg. Chem.* **2011**, *50*, 7229−7238.

(43) Glusac, K. D.; Jiang, S. J.; Schanze, K. S. *Chem. Commun.* **2002**, 2504−2505.

(44) Zeng, X.; Tavasli, M.; Perepichka, I.; Batsanov, A.; Bryce, M.; Chiang, C.; Rothe, C.; Monkman, A. P. *Chem.—Eur. J.* **2008**, *14*, 933−943.

(45) Kim, K. Y.; Farley, R. T.; Schanze, K. S. *J. Phys. Chem. B* **2006**, *110*, 17302−17304.

(46) Dragonetti, C.; Righetto, S.; Roberto, D.; Ugo, R.; Valore, A.; Fantacci, S.; Sgamellotti, A.; De Angelis, F. *Chem. Commun.* **2007**, 4116−4118.

(47) Valore, A.; Cariati, E.; Dragonetti, C.; Righetto, S.; Roberto, D.; Ugo, R.; De Angelis, F.; Fantacci, S.; Sgamellotti, A.; Macchioni, A.; Zuccaccia, D. *Chem.—Eur. J.* **2010**, *16*, 4814−4825.

(48) De Angelis, F.; Fantacci, S.; Evans, N.; Klein, C.; Zakeeruddin, S. M.; Moser, J. E.; Kalyanasundaram, K.; Bolink, H. J.; Gratzel, M.; Nazeeruddin, M. K. *Inorg. Chem.* **2007**, *46*, 5989−6001.

(49) Wu, S.; Ling, J.; Lai, S.; Huang, M.; Cheng, C.; Chen, I. *J. Phys. Chem. A* **2010**, *114*, 10339−10344.

(50) Rogers, J. E.; Slagle, J. E.; Krein, D. M.; Burke, A. R.; Hall, B. C.; Fratini, A.; McLean, D. G.; Fleitz, P. A.; Cooper, T. M.; Drobizhev, M.; Makarov, N. S.; Rebane, A.; Kim, K. Y.; Farley, R.; Schanze, K. S. *Inorg. Chem.* **2007**, *46*, 6483−6494.

(51) Kim, S. O.; Zhao, Q.; Thangaraju, K.; Kim, J. J.; Kim, Y. H.; Kwon, S. K. *Dyes Pigm.* **2011**, *90*, 139−145.

(52) Mauro, M.; De Paoli, G.; Otter, M.; Donghi, D.; D'Alfonso, G.; De Cola, L. *Dalton Trans.* **2011**, *40*, 12106−12116.

(53) Demas, J. N.; Crosby, G. A. *J. Phys. Chem.* **1971**, *75*, 991−1024.

(54) Vanhouten, J.; Watts, R. J. *J. Am. Chem. Soc.* **1976**, *98*, 4853−4858.

(55) Carmichael, I.; Hug, G. L. *J. Phys. Chem. Ref. Data* **1986**, *15*, 1−250.

(56) Kumar, C. V.; Qin, L.; Das, P. K. *J. Chem. Soc., Faraday Trans. 2* **1984**, *80*, 783−793.

(57) Liu, R.; Azenkeng, A.; Zhou, D.; Li, Y.; Glusac, K. D.; Sun, W. *J. Phys. Chem. A* **2013**, *117*, 1907−1917.

(58) Frisch, M. J.; Trucks, G. W.; Schlegel, H. B.; Scuseria, G. E.; Robb, M. A.; Cheeseman, J. R.; Scalmani, G.; Barone, V.; Mennucci, B.; Petersson, G. A.; Nakatsuji, H.; Caricato, M.; Li, X.; Hratchian, H. P.; Izmaylov, A. F.; Bloino, J.; Zheng, G.; Sonnenberg, J. L.; Hada, M.; Ehara, M.; Toyota, K.; Fukuda, R.; Hasegawa, J.; Ishida, M.; Nakajima, T.; Honda, Y.; Kitao, O.; Nakai, H.; Vreven, T.; Montgomery, J. A., Jr.; Peralta, J. E.; Ogliaro, F.; Bearpark, M.; Heyd, J. J.; Brothers, E.; Kudin, K. N.; Staroverov, V. N.; Kobayashi, R.; Normand, J.; Raghavachari, K.; Rendell, A.; Burant, J. C.; Iyengar, S. S.; Tomasi, J.; Cossi, M.; Rega, N.; Millam, J. M.; Klene, M.; Knox, J. E.; Cross, J. B.; Bakken, V.; Adamo, C.; Jaramillo, J.; Gomperts, R.; Stratmann, R. E.; Yazyev, O.; Austin, A. J.; Cammi, R.; Pomelli, C.; Ochterski, J. W.; Martin, R. L.; Morokuma, K.; Zakrzewski, V. G.; Voth, G. A.; Salvador, P.; Dannenberg, J. J.; Dapprich, S.; Daniels, A. D.; Farkas, O.; Foresman, J. B.; Ortiz, J. V.; Cioslowski, J.; Fox, D. J. *Gaussian 09*, revision A.1; Gaussian, Inc.: Wallingford, CT, 2009.

(59) Perdew, J. P.; Burke, K.; Ernzerhof, M. *Phys. Rev. Lett.* **1996**, *77*, 3865−3868.

(60) Adamo, C.; Barone, V. *J. Chem. Phys.* **1999**, *110*, 6158−6170.

(61) Hay, P. J.; Wadt, W. R. *J. Chem. Phys.* **1985**, *82*, 299−310.

(62) Krishnan, R.; Binkley, J. S.; Seeger, R.; Pople, J. A. *J. Chem. Phys.* **1980**, *72*, 650−654.

(63) Hariharan, P. C.; Pople, J. A. *Theor. Chim. Acta* **1973**, *28*, 213−222.

(64) Clark, T.; Chandrasekhar, J.; Spitznagel, G. W.; Schleyer, P. v. R. *J. Comput. Chem.* **1983**, *4*, 294−301.

(65) Francl, M. M.; Pietro, W. J.; Hehre, W. J.; Binkley, J. S.; Gordon, M. S.; DeFrees, D. J.; Pople, J. A. *J. Chem. Phys.* **1982**, *77*, 3654−3665.

(66) Gill, P. M. W.; Johnson, B. G.; Pople, J. A.; Frisch, M. J. *Chem. Phys. Lett.* **1992**, *197*, 499−505.

(67) Barone, V.; Cossi, M.; Tomasi, J. *J. Comput. Chem.* **1998**, *19*, 404−417.

(68) Cossi, M.; Rega, N.; Scalmani, G.; Barone, V. *J. Comput. Chem.* **2003**, *24*, 669−681.

(69) Scalmani, G.; Frisch, M. J.; Mennucci, B.; Tomasi, J.; Cammi, R.; Barone, V. *J. Chem. Phys.* **2006**, *124*, 094107−1−094107−15.

(70) Furche, F.; Ahlrichs, R. *J. Chem. Phys.* **2002**, *117*, 7433−7447.

(71) Martin, R. L. *J. Chem. Phys.* **2003**, *118*, 4775−4777.

(72) Badaeva, E.; Albert, V. V.; Kilina, S.; Koposov, A.; Sykora, M.; Tretiak, S. *Phys. Chem. Chem. Phys.* **2010**, *12*, 8902−8913.

(73) Batista, E. R.; Martin, R. L. *J. Phys. Chem. A* **2005**, *109*, 9856−9859.

(74) Gahungu, G.; Su, J.; Qu, X.; Liu, Y.; Si, Y.; Shang, X.; Wu, Z. *Dalton Trans.* **2012**, *41*, 10228−10237.

(75) Dennington, R., II; Keith, T.; Millam, J. *GaussView*; Semichem Inc.: Shawnee Mission, KS, 2007.

(76) Nonoyama, M. B. *Bull. Chem. Soc. Jpn.* **1974**, *47*, 767−768.

(77) Firey, P. A.; Ford, W. E.; Sounik, J. R.; Kenney, M. E.; Rodgers, M. A. J. *J. Am. Chem. Soc.* **1988**, *110*, 7626−7630.

(78) Lamansky, S.; Djurovich, P.; Murphy, D.; Abdel-Razzaq, F.; Lee, H. E.; Adachi, C.; Burrows, P. E.; Forrest, S. R.; Thompson, M. E. *J. Am. Chem. Soc.* **2001**, *123*, 4304−4312.

(79) Reichardt, C. *Chem. Rev.* **1994**, *94*, 2319−2358.

(80) Pomestchenko, I. E.; Castellano, F. N. *J. Phys. Chem. A* **2004**, *108*, 3485−3492.

(81) Liu, R.; Li, Y.; Li, Y.; Zhu, H.; Sun, W. *J. Phys. Chem. A* **2010**, *114*, 12639−12645.

(82) Lafolet, F.; Welter, S.; Popovic, Z.; De Cola, L. *J. Mater. Chem.* **2005**, *15*, 2820−2828.

(83) Ichimura, K.; Kobayashi, T.; King, K. A.; Watts, R. J. *J. Phys. Chem.* **1987**, *91*, 6104−6106.

(84) Liu, S.; Schanze, K. S. *Chem. Commun.* **2004**, 1510−1511.

(85) Sun, Y.; Joyce, L. E.; Dickson, N. M.; Turro, C. *Chem. Commun.* **2010**, *46*, 2426−2428.

(86) Shaw, J. R.; Webb, R. T.; Schmehl, R. H. *J. Am. Chem. Soc.* **1990**, *112*, 1117−1123.

(87) Tyson, D. S.; Luman, C. R.; Zhou, X.; Castellano, F. N. *Inorg. Chem.* **2001**, *40*, 4063−4071.

(88) Dubinina, G. G.; Price, R. S.; Abboud, K. A.; Wicks, G.; Wnuk, P.; Stepanenko, Y.; Drobizhev, M.; Rebane, A.; Schanze, K. S. *J. Am. Chem. Soc.* **2012**, *134*, 19346−19349.

(89) Li, Y.; Liu, R.; Badaeva, E.; Kilina, S.; Sun, W. *J. Phy. Chem. C* **2013**, *117*, 5908−5918.

(90) Zhang, B.; Li, Y.; Liu, R.; Pritchett, T. M.; Haley, J. E.; Sun, W. *ACS Appl. Mater. Interfaces* **2013**, *5*, 565−572.

(91) McKay, T. J.; Staromlynska, J.; Davy, J. R.; Bolger, J. A. *J. Opt. Soc. Am. B* **2001**, *18*, 358−362.

(92) Shao, P.; Li, Y.; Yi, J.; Pritchett, T. M.; Sun, W. *Inorg. Chem.* **2010**, *49*, 4507−4517.

(93) Li, Y.; Pritchett, T.; Shao, P.; Haley, J.; Zhu, H.; Sun, W. *J. Organomet. Chem.* **2009**, *694*, 3688−3691.

(94) Ji, Z.; Li, Y.; Sun, W. *Inorg. Chem.* **2008**, *47*, 7599−7607.

(95) Pritchett, T. M.; Sun, W.; Guo, F.; Zhang, B.; Ferry, M. J.; Rogers-Haley, J. E.; Shensky, W.; Mott, A. G. *Opt. Lett.* **2008**, *33*, 1053−1055.

(96) Li, Y.; Pritchett, T. M.; Huang, J.; Ke, M.; Shao, P.; Sun, W. *J. Phys. Chem. A* **2008**, *112*, 7200−7207.

(97) Shao, P.; Li, Y.; Sun, W. *J. Phys. Chem. A* **2008**, *112*, 1172−1179.

(98) Sun, W.; Zhu, H.; Barron, P. M. *Chem. Mater.* **2006**, *18*, 2602−2610.

(99) Guo, F.; Sun, W.; Liu, Y.; Schanze, K. *Inorg. Chem.* **2005**, *44*, 4055−4065.

(100) Perry, J. W.; Mansour, K.; Lee, I. Y. S.; Wu, X.; Bedworth, P. V.; Chen, C.; Ng, D.; Marder, S. R.; Miles, P.; Wada, T.; Tian, M.; Sasabe, H. *Science* **1996**, *273*, 1533−1536.

(101) Song, Y.; Fang, G.; Wang, Y.; Liu, S.; Li, C.; Song, L.; Zhu, Y.; Hu, Q. *Appl. Phys. Lett.* **1999**, *74*, 332−334.

(102) Pittman, M.; Plaza, P.; Martin, M. M.; Meyer, Y. H. *Opt. Commun.* **1998**, *158*, 201−212.

(103) Guha, S.; Kang, K.; Porter, P.; Roach, J. E.; Remy, D. E.; Aranda, F. J.; Rao, D. V. G. L. N. *Opt. Lett.* **1992**, *17*, 264−266.

(104) Ji, Z.; Li, Y.; Pritchett, T. M.; Makarov, N. S.; Haley, J. E.; Li, Z.; Drobizhev, M.; Rebane, A.; Sun, W. *Chem.—Eur. J.* **2011**, *17*, 2479−2491.

(105) Shao, P.; Li, Y.; Sun, W. *Organometallics* **2008**, *27*, 2743−2749.

6570

dx.doi.org/10.1021/am401133p | *ACS Appl. Mater. Interfaces* 2013, 5, 6556−6570